Manuscript prepared for Atmos. Chem. Phys.
with version 2014/09/16 7.15 Copernicus papers of the LaTeX class copernicus.cls.
Date: 28 July 2017

Reconciling differences in stratospheric ozone composites

William T. Ball[1,2], Justin Alsing[3,4], Daniel J. Mortlock[4,5,6], Eugene V. Rozanov[1,2], Fiona Tummon[1], and Joanna D. Haigh[4,7]

[1]Institute for Atmospheric and Climate Science, Swiss Federal Institute of Technology Zurich, Universitaetstrasse 16, CHN, CH-8092 Zurich, Switzerland
[2]Physikalisch-Meteorologisches Observatorium Davos World Radiation Centre, Dorfstrasse 33, 7260 Davos Dorf, Switzerland
[3]Center for Computational Astrophysics, Flatiron Institute, 162 5th Ave, New York, NY 10010, USA
[4]Physics Department, Blackett Laboratory, Imperial College London, SW7 2AZ, UK
[5]Department of Mathematics, Imperial College London, SW7 2AZ, UK
[6]Department of Astronomy, Stockholms universitet, SE-106 91 Stockholm, Sweden
[7]Grantham Institute - Climate Change and the Environment, Imperial College London, SW7 2AZ, UK

Correspondence to: W. T. Ball (william.ball@env.ethz.ch)

Abstract.

Observations of stratospheric ozone from multiple instruments now span three decades; combining these into composite datasets allows long-term ozone trends to be estimated. Recently, several ozone composites have been published, but trends disagree by latitude and altitude, even between composites built upon the same instrument data. We confirm that the main causes of differences in decadal trend estimates lie in (i) steps in the composite timeseries when the instrument source data changes and (ii) artificial sub-decadal trends in the underlying instrument data. These artefacts introduce features that can alias with regressors in multiple linear regression (MLR) analysis; both lead to inaccurate trend estimates. **Here, we aim to remove these artefacts by inferring using Bayesian methods to infer the underlying ozone timeseries from a set of composites by building a joint-likelihood function for the set of composites using a Gaussian-mixture density to model outliers introduced by data-artefacts, together with a data-driven prior on ozone variability incorporating knowledge of problems during instrument operation**. We apply **this Bayesian self-calibration approach** to stratospheric ozone in 10° bands from 60°S–60°N and from 46–1 hPa (~21–48 km) for 1985–2012. There are two main outcomes: (i) we independently identify and confirm many of the data problems previously identified, but which remain unaccounted for in existing composites; (ii) we construct an ozone composite, with uncertainties, that is free from most of these problems**; we call this the BAyeSian Integrated and Consolidated (BASIC) composite**. After constructing the new BASIC composite, to analyse the new composite we use dynamical lin-

ear modeling (DLM), which provides a more robust estimate of long-term changes through Bayesian inference than MLR. **BASIC** and DLM, together, provide a step forward in improving estimates of decadal trends. Our results indicate a significant recovery of ozone since 1998 in the upper stratosphere, of both northern and southern mid-latitudes, in all four composites analysed, and particularly in the BASIC composite. The **BASIC** results also show no hemispheric difference in the recovery at mid-latitudes, in contrast to an apparent feature that is present, but not consistent, in the four composites. **Our overall conclusion is that it is possible to effectively combine different ozone composites and account for artefacts and drifts, and that this leads to a clear and significant result that upper stratospheric ozone levels have increased since 1998, following an earlier decline.**

1   Introduction

The ozone layer in the stratosphere protects the Earth's biosphere from harmful solar ultra-violet (UV) radiation. The use ozone depleting substances (ODSs), including chloro-flurocarbons (CFCs), led to a decline in ozone globally over the latter half of the 20th Century (Johnston, 1971; Crutzen, 1971; Molina and Rowland, 1974), particularly in the polar regions (WMO, 2011, 2014). The implementation of the Montreal Protocol (MP), which banned the use of most ODSs, has halted this decline and in some regions there has been a recovery in total column ozone (Solomon et al., 2016). However, there is large uncertainty in the sign and magnitude of recent trends depending on altitude and latitude, and a clear signal is difficult to determine (Harris et al., 2015).

Ozone responds to forcings from below, e.g. injections of aerosols from volcanoes (Robock, 2000) or wave activity from the troposphere (Kidston et al., 2015), and from above, e.g. from solar sources such as UV radiation (Haigh, 1994) and particles (Funke et al., 2011; Mironova et al., 2015). In order to quantify and understand the variability forced by a particular driver, and long-term trends in ozone - not just in terms of the total column ozone (TCO), but also resolved vertical profiles - observations spanning multiple decades are needed. Such a dataset can only be provided by combining data from multiple sources (Harris et al., 2015; Tummon et al., 2015). The method used to combine the data needs to consider different inherent attributes, the most important of which include: temporal resolution; vertical and horizontal spatial resolution (Kramarova et al., 2013a); time of day and geolocation of observations (Sofieva et al., 2014); absolute calibration (Frith et al., 2014); and stability estimates and instrument uncertainty (DeLand et al., 2012); All of these factors, if not well accounted for, can introduce additional (artificial) trends, uncertainties and errors, which may leak into statistical analyses of decadal trends (Harris et al., 2015; Tummon et al., 2015) and estimates of the magnitude of the response to drivers such as the Sun (Maycock et al., 2016). This can lead to conflicting results from different datasets (WMO, 2014).

Observational records of atmospheric ozone began with ground-based observations in 1921 (Stae-helin et al., 1998) and were joined by satellite observations in the 1960s (Krueger et al., 1980). These records are an invaluable tool to understand not only the long-term trends in ozone, but also how the middle atmosphere operates. Ground-based observations have the advantage of being longer records and can be re-calibrated on a continuous basis, but they are point-source observations and thus cannot account for large differences in ozone concentration and variability with latitude and longitude. The introduction of satellite observations have allowed for near-global, continuous observations over many decades, but has the disadvantages of typically only operating for a limited number of years and being subject to space-based degradation.

Creating an accurate record of stratospheric ozone profiles is a non-trivial task and much work has been done at every stage, from design, construction and during flight, to post-processing and combining datasets into composites (Kyrölä et al., 2013; McPeters et al., 2013; Sofieva et al., 2013; Sioris et al., 2014; Froidevaux et al., 2015; Davis et al., 2016). Recently, several composites were published by multiple groups in connection with the SI2N initiative (SPARC (Stratosphere-troposphere Processes And their Role in Climate)/IO3C (International Ozone Commission)/IGACO-O3 (Integrated Global Atmospheric Chemistry Observations – Ozone)/NDACC (Network for the Detection of Atmospheric Composition Change)) (Tummon et al., 2015). Nevertheless, even when problems are flagged, and uncertainties are minimized, the fact that different composites lead to trend estimates that differ by more than their uncertainties (e.g. Fig. 6 of Harris et al., 2015 and Fig. 8 of Tummon et al., 2015) means that at least one, if not all, are insufficiently stable during some periods to provide a robust estimate of changes in ozone throughout the stratosphere. Tummon et al. (2015) further notes that the choice of instruments to merge has more impact on trends than the merging technique used, that the construction approach needs careful consideration of the method used to avoid contaminating trends with artefacts, and that so far it has not been possible to remove biases from any individual, vertically-resolved, dataset.

Despite these difficulties, it is possible to account for many of these problems. There is common information within all the composites, e.g. the annual variability is similar in most composites (Tummon et al., 2015), and the differences between composite datasets due to the issues listed above should, in principle, point to where potential artefacts such as steps and drifts are located in time and by latitude and altitude. This can be especially effective in the case of an unexpected or erroneous change occurring in one dataset, which is absent in all the others. Once the instrument or composite at fault is identified, there is the possibility of flagging, removing or rectifying an error, and confidence in applying a correction increases if the deviation or fault can be linked to a known issue. Thus, together with this prior knowledge and an unbiased uncertainty estimate, one can evaluate the likelihood of an observation being correct or, indeed, estimate the most likely value.

Our goal here is to provide a technique whereby the most likely ozone variability throughout the stratosphere can be identified by using the information embedded within multiple datasets si-

multaneously. The natural approach with which to tackle such a problem is using Bayesian inference (Cox, 1946; Lee et al., 2005; Arnold et al., 2007). **In adopting a Bayesian approach, we develop a detailed probabilistic model for the (multiple) datasets, carefully allowing for outliers and accounting for all knowledge (and ignorance) of measurement uncertainties and any known problems during instrument operation. Additionally, by incorporating (data-driven) prior information about the underlying ozone variability, we are able to identify - using only the data and knowledge of the instruments - where some datasets are systematically biased due to measurement artefacts whilst others are consistent with the anticipated month-to-month variability. In this way, our approach combines the multiple datasets in such a way that they "self-calibrate" each other, resulting in a single ozone timeseries that is cleaned of many of the artefacts affecting any individual dataset (although if a problem is common to all datasets, it cannot be identified).**

This paper has three main parts. In the first (section 2), we introduce the composite datasets we use (section 2.1) by explicitly presenting the problems we will later attempt to fix. Ozone composites have been updated since important inter-comparison papers by Harris et al. (2015) and Tummon et al. (2015) , so our results cannot be directly compared with theirs; we briefly present some of these differences (section 2.2). The ozone composites, described in section 2, form a good starting point from which to combine information and account for differences, since the effort put into producing them already considers and accounts for many instrument and observational issues. However, some remaining problems are clear in the composites. In the second part, we present the Bayesian method to self-correct the ozone composites (section 3), construct uncertainty estimates (section 3.1), **form the Gaussian-mixture likelihood (section 3.2)**, develop transition-priors to estimate how ozone is expected to vary on monthly timescales (section 3.3) and discuss how we include additional prior information that we have available (section 3.1). **We call this combined set of steps and algorithms the BAyeSian Integrated and Consolidated (BASIC) approach.** The resulting BASIC composite timeseries are presented and compared with the composites in sections 4.2 and 4.3. In the final part (section 5), we primarily use dynamical linear modeling (DLM) to evaluate long-term trends (section 5.2), although we compare our results with multiple linear regression (MLR) analysis, and present our results for ozone changes over the 1985-2012 period in section 5.3. We conclude in section 6.

2 Data

2.1 Ozone composites

The SI2N project promoted seven ozone composites of satellite observations, summarised in Tummon et al. (2015), along with detailed comparisons that were expanded upon by Harris et al. (2015). Three of the datasets, named SAGE-GOMOS1 (Kyrölä et al., 2013), SAGE-GOMOS2 (Tummon

et al., 2015) and SAGE-OSIRIS (Adams et al., 2014) in Tummon et al. (2015), have more data missing than the others (~57% for 1985–2012 for 20°S—20°N), so we do not consider them in our analysis. Two of the remaining composites have the SAGE-II instrument (Stratospheric Aerosol and Gas Experiment II) (Damadeo et al., 2013) as a backbone: GOZCARDS (Global OZone Chemistry

130 And Related Datasets for the Stratosphere; Froidevaux et al. (2015)) and SWOOSH (Stratospheric Water and Ozone Satellite Homogenized; Davis et al. (2016)); we will refer to this pair of composites as 'SAGE-based'. The other two 'SBUV-based' composites we consider use the suite of SBUV-type (Solar-Backscatter Ultraviolet) instruments: SBUV-MOD (SBUV Version 8.6 Merged Ozone Data Set; Frith et al. (2014)) and SBUV-MER (SBUV Merged Cohesive; Wild and Long (2017)). By

135 using only two pairs of composites containing approximately equal weighting, we partly avoid the issue of biasing results to SAGE-based composites, a concern raised in the analysis of Harris et al. (2015) (though see appendix A5.2).

We consider zonal-mean, monthly-mean ozone over the 28-year period, January 1985 – December 2012, covered by all datasets. While the correction method we present later (section 3) could, in

140 principle, be used to deal with data gaps at higher latitudes, we limit our latitude range to twelve 10° bands over 60°S—60°N. We limit the pressure range to 11 levels from 46–1 hPa (~21–48 km) to avoid issues of large diurnal variations at higher altitudes, and because the vertically resolved SBUV data are not available at lower altitudes (i.e. at higher pressures); **note, however, that some diurnal variability exists down to 5 hPa.** In order to treat each composite fairly, we interpolate

145 all four onto the GOZCARDS pressure–latitude grid since this grid has the lowest resolution of the four (though the instruments themselves have a higher resolution); a visualization of the original grids are shown in appendix Fig. A1. All considered composites have data available for more than 80% of all months at most latitudes. Finally, for this work, we are interested in relative variability and trends, so we shift absolute values to agree with the mean of SWOOSH from August 2005

150 to December 2012 when the Aura/MLS instrument is used; during this period all the composites show remarkably good agreement on annual and multi-year timescales, and regression coefficients using multiple linear regression (see section 5.1) are similar at all pressure levels and latitudes (not shown). This is important since a common reference period we trust improves the ability for the **BASIC approach** to estimate relative changes and reduces uncertainties.

155 The ozone instrument data and composites are already extensively detailed and discussed in several recent papers as listed above, e.g. Tummon et al. (2015); Harris et al. (2015); we recommend that interested readers consult these, which also include an exhaustive list of references to individual instruments. We will discuss relevant points of interest regarding each composite in the discussion that follows below.
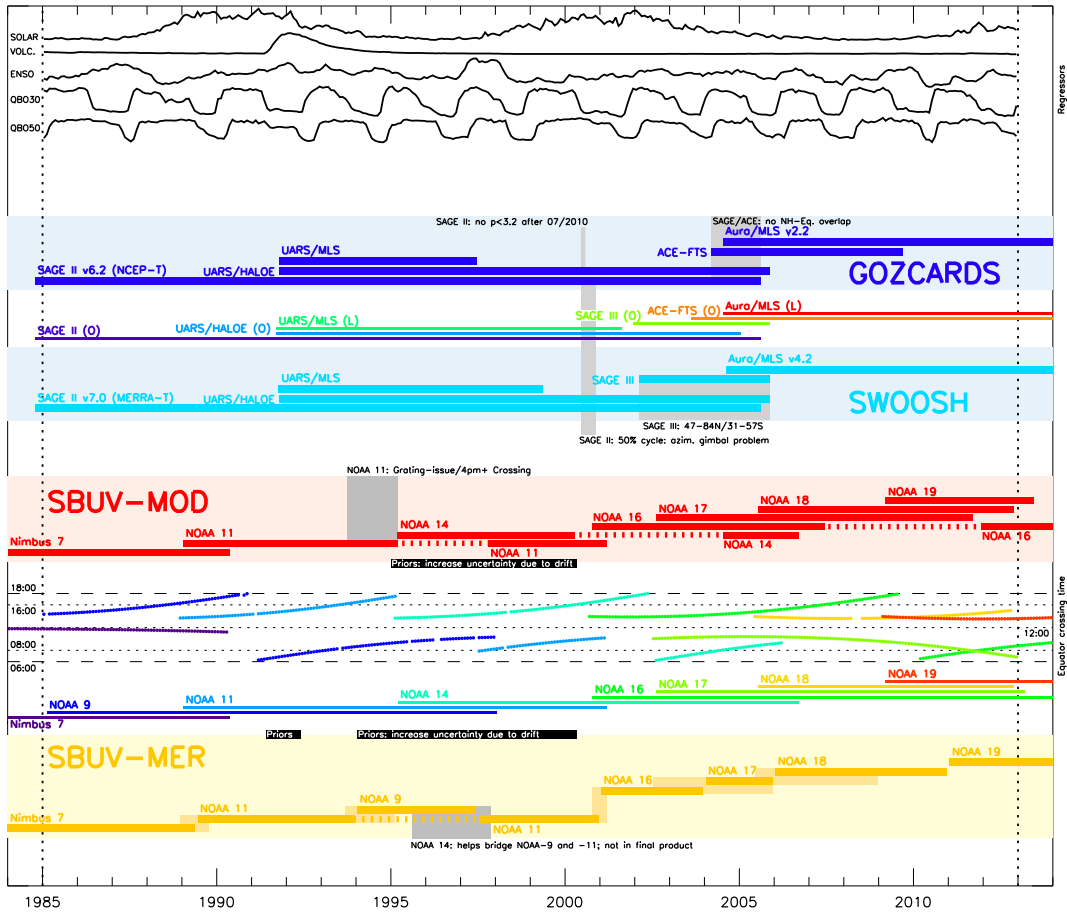
Figure 1: A guide to the regression indices used in the trend analysis (upper third) and instrument data used to construct SAGE-based (middle third: GOZCARDS, dark blue; SWOOSH, light blue) and SBUV-based (lower third: SBUV-MOD, red; SBUV-MER, yellow) composites. Shading at SBUV-MER instrument changes indicate periods used to determine differences in annual variability by applying bias corrections between instruments. The full periods of instrument operation for datasets in these pairs are shown with multiple colours between the composites. Where SBUV data are not used for an interval, dashed lines replace solid. Between the SBUV-composites, the local-time of equator crossing is shown. Where relevant, version numbers are given with instrument names; 'O' and 'L' indicate the satellite was a limb-viewer or occultation-based instrument; SBUV instruments are all nadir-viewing. Grey-shading with black text highlights periods discussed in the article. Periods specifically flagged to increase the SBUV uncertainty estimates in the **BASIC approach** are labelled black with white text.
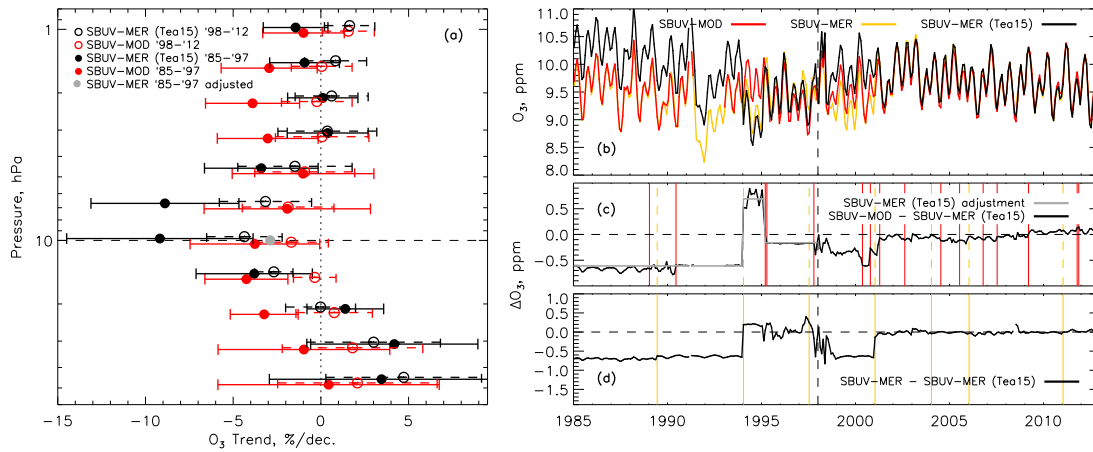
Figure 2: (**a**) The equatorial (20°S–20°N) decadal ozone MLR trend profiles for SBUV-MER version used by Tummon et al. (2015) ('Tea15'; black) and SBUV-MOD (red). Dots and solid error bars represent the 1985–1997 trends, and open circles and dashed error bars the 1998–2012 period. A single grey dot is plotted at 10 hPa, which follows an adjustment to SBUV-MER as shown in (c) as a grey line. (**b**) The ozone composite timeseries for SBUV-MER–Tea15 (black), SBUV-MER (yellow) and SBUV-MOD (red) at 10 hPa, all shifted to the July 2005 — 2012 mean of SWOOSH. (**c**) The difference between the SBUV-MOD and -MER-Tea15 timeseries in (b); the grey line prior to 1998 is a correction applied to SBUV-MER–Tea15 to produce the grey dot in (a). (**d**) The difference between SBUV-MER–Tea15 and SBUV-MER. The vertical dashed line in (b–d) indicates 1 January 1998, which delimits the two periods considered in the MLR results in (a). Error bars are 2σ.

2.2 Inconsistencies between composites

To determine why decadal trends from the various composites are different requires an understanding of how they have been constructed with satellite instrument data from multiple sources. We present a visual reference guide for the four composites in Fig. 1. Here, we show the time-line of instruments used to construct the SAGE-based data in the middle, and SBUV below. The colour-coding for the four datasets (GOZCARDS dark blue, SWOOSH light blue, SBUV-MOD red, SBUV-MER yellow) will be used throughout the paper. The operating periods of all the instrument datasets used for either SWOOSH or GOZCARDS are presented as a spectrum of colours between them; the same is done for the SBUV-composites, where we additionally show information related to the time of day at which equator-crossings occur, which will be important later. Instrument names are given near the start of their operation period. Various comments and grey-shadings litter the plot; these mark points to be aware of and some of these are discussed later.

2.2.1 SBUV-based composites

The two SBUV-composites are built in two different ways: SBUV-MER uses overlapping timeseries (shading in Fig. 1) to calculate offsets (calibration biases) and differences in seasonal and diurnal

175 variation, but only a single dataset is used without averaging overlapping periods; SBUV-MOD also accounts for offsets, but then overlapping data are averaged. SBUV-MOD relies on the instrument to instrument calibration done at the wavelength level within the version 8.6 algorithm for absolute calibration (i.e. no additional offsets are applied before averaging).

The SBUV-based composites use only instruments with the same design and are the longest single-
180 instrument-type composites available. Both use the same NOAA and Nimbus space-based platforms, though not always at the same time, except that SBUV-MER uses NOAA-9 observations between 1994 and 1997 to increase global coverage and bridge the gap in NOAA-11 (Fig. 1), which is an update to SBUV-MER that differs from the previous version considered by Tummon et al. (2015) (see below); **SBUV-MER also uses NOAA-14 as a backbone to connect biases in NOAA-9 and**
185 **-11, but the NOAA-14 data itself are not used in the final product**. The SBUV instruments infer profile ozone in units of parts per million (ppm) volume mixing ratio from measurements of back-scattered UV radiation at wavelengths shorter than 300 nm in a downward, nadir viewing system, which is fundamentally different from the limb/occultation instruments used in the SAGE-based composites; the SBUV instruments are optimised to low stray-light and high signal-to-noise radi-
190 ance measurements, with an estimated accuracy of 1–2 DU at solar zenith angles up to 70 degrees (McPeters et al., 2013). Despite being constructed with essentially the same instrument data, the two datasets show differences in estimated decadal trends (Harris et al., 2015; Tummon et al., 2015).

In Fig. 2a, we recreate the SBUV-MOD and SBUV-MER 1985–1997 (dots and solid lines) and 1998–2012 (circles and dashed lines) linear decadal ozone trend estimates from MLR (section 5.1)
195 for the equatorial regions 20°S–20°N as in Figs. 5 and 6 of Harris et al. (2015) and Fig. 8 of Tummon et al. (2015). SBUV-MER has seen revisions since it was used in Harris et al. (2015) and Tummon et al. (2015), so we use the version in those publications to make clear why previous analyses of the SBUV-composites differ (labelled 'Tea15'); after this section we only consider the latest update. The two composites show good agreement over the 1998–2012 period in both mean value and profile
200 shape. The earlier period shows different vertical structure; at 10 hPa the mean values disagree by more than 5% per decade (the 10 hPa level is indicated by the horizontal dashed line). The reason for this becomes obvious when we plot the absolute, and differences of, the timeseries at 10 hPa in Fig. 2b and c, respectively. Prior to 2002, the difference between SBUV-MER (Tea15) and SBUV-MOD can be almost as large as the annual variability. Fig. 2c reveals that these are caused by steps,
205 of which the two largest occur in January 1994 and February–April 1995. We plot coloured vertical lines when instruments in either composite change (yellow for SBUV-MER, red for SBUV-MOD), which immediately reveals that these jumps are related to offsets in instrument data: the first occurred in SBUV-MER, the second in SBUV-MOD. To prove it is these steps that cause the difference in the pre-1998 trend estimated at 10 hPa in Fig. 2a, we simply subtract the grey curve indicated in Fig. 2c
210 from SBUV-MER (Tea15) and the mean MLR estimate for the trend is indicated as a grey-dot in
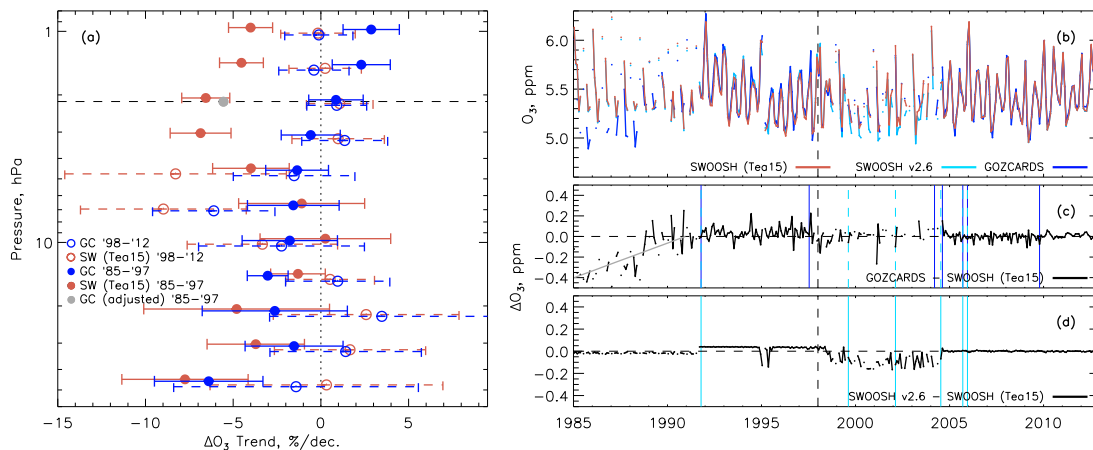
Figure 3: (**a**) The equatorial (20°S–20°N) decadal ozone MLR trend profiles for SWOOSH from Tummon et al. (2015) ('Tea15'; red) and GOZCARDS (blue). Dots and solid error bars represent the 1985–1997 trends, and open circles and dashed error bars the 1998–2012 period. A single grey dot is plotted at 2.2 hPa, which follows an adjustment to SWOOSH (Tea15) as shown in (c) as a grey line. (**b**) The ozone composite timeseries for SWOOSH–Tea15 (black), SWOOSH v2.6 (light-blue) and GOZCARDS (blue) at 2.2 hPa, all shifted to the July 2005–2012 mean of SWOOSH v2.6. (**c**) The difference between the GOZCARDS and SWOOSH–Tea15 timeseries in (b); the grey line prior to 1991 is an adjustment applied to GOZCARDS to produce the grey dot in (a). (**d**) The difference of SWOOSH-Tea15 and SWOOSH v2.6. The vertical dashed line in (b–d) indicates 1 January 1998, which delimits the two periods considered in the MLR results in (a). Error bars are 2σ.

Fig. 2a, now very close to SBUV-MOD. We note that this subtraction is not intended to indicate that SBUV-MOD is correct, but is a simple test to understand why the trends differ.

Fig. 2d shows the difference between SBUV-MER (Tea15) and the updated version, which shows many of the offsets relative to SBUV-MOD in Fig. 2c have been removed. However, artefacts still remain in the newer version with respect to SBUV-MOD, and we find that they are not confined just to the altitude and latitude-range shown in these plots. Ultimately, the remaining differences lead to the divergent trend estimates. We return to this in section 4.3; further discussion on the SBUV-composites is provided in Appendix A1.

2.2.2 SAGE-based composites

While constructed by two separate teams, GOZCARDS (Froidevaux et al., 2015) and SWOOSH (Davis et al., 2016) are similar for two main reasons: (i) the longest single instrument record used is SAGE-II (1984–2005) and this acts as the absolute reference level in both datasets; and (ii) they are constructed from limb-viewers and occultation satellites (identified as 'L' and 'O' in Fig. 1), meaning they differ in operation from the SBUV-nadir viewers. Occultation satellites measure ozone by looking at the disk of the rising or setting Sun though the atmosphere (SAGE-II uses the UV and visible, while e.g. HALOE and ACE-FTS use infra-red wavelengths); this makes their vertical

profile resolution higher, but at the expense of only observing 15 profiles per day. Limb sounders observe thermal emission in the infra-red or microwave as volume mixing ratio on pressure levels and can observe thousands of profiles each day. The composites differ in several ways, most relevant of

230 which are: (i) they use different data screening and pre-processing; (ii) data from the same satellites are used for different periods and/or spatial regions; (iii) SWOOSH contains SAGE-III data and not ACE-FTS observations, and GOZCARDS vice-versa (see Fig. 1); and (iv) GOZCARDS uses SAGE-II version 6.2, while SWOOSH uses version 7.0 – this innocuous difference has consequences for the trends (and solar signal analysis; not shown) that we will elaborate on in the following.

235 Because SAGE-II observes ozone number density, knowledge of local temperature is needed to convert to volume mixing ratio. GOZCARDS uses SAGE-II v6.2, and SWOOSH SAGE-II v7.0; the former uses NCEP reanalysis temperatures while the latter uses the MERRA reanalysis (see Damadeo et al. (2013) and references within). It has been noted by McLinden et al. (2009), and confirmed by Maycock et al. (2016), that the NCEP temperature data contain spurious trends. The

240 fact that the trend is not visible in SBUV data (section 4.3) further supports this. The impact of the different versions of SAGE-II within the SAGE-based composites is shown in Fig. 3. We note that, as for SBUV-MER, the current SWOOSH release has changed with respect to the aforementioned publications. Therefore, we again initially show results from the earlier version (2.1) in red (again designated 'Tea15'); following this discussion we will not refer to this version again. Fig. 3a shows

245 the equatorial (20°S–20°N) decadal ozone trends similar to Fig. 2 extracted from GOZCARDS and SWOOSH (Tea15) using MLR for two periods: 1985–1997 (dots and solid lines) and 1998–2012 (circles and dashed lines). We see that for 1998–2012, except at 4.6 and 6.8 hPa, the two mean profiles agree well. However, for 1985–1997 above 5 hPa the ozone profiles show very large differences. To clarify why, in Fig. 3b we plot their 2.2 hPa timeseries, and their difference in Fig. 3c; the

250 vertical dashed line indicates where the two periods considered in Fig. 3a are delimited. After 1991, both composites show similar long-term variability, though there are clearly sub-periods containing different scatter characteristics, and which change between instrument periods (vertical coloured lines), thus indicating a relationship to either different pre-processing or instrument usage. Between 1985 and 1991, GOZCARDS is lower than SWOOSH, and there appears to be an approximately lin-

255 ear increase over this period. Similar to the approach taken for SBUV-MER in Fig. 2, correcting the 1985–1991 period with a simple linear trend-line (grey in Fig. 3c) leads to very good agreement with SWOOSH (Tea15) in Fig. 3a (grey dot), showing the difference between the two SAGE-composites at 2.2 hPa is mainly caused by the pre-1991 drift in GOZCARDS; this is a result of the conversion of SAGE-II version 6.2 data (used in GOZCARDS) from densities to mixing ratios using NCEP

260 temperatures, while the version 7 SAGE-II dataset (used in SWOOSH) uses MERRA and thereby corrects this issue.

Finally, we show in Fig. 3d the difference between SWOOSH (Tea15) and the latest version (2.6), which sees only minor step changes and short-term variance that appears to line up with instrument

changes, except for between 1998 and 2004. Again, it is not clear from this difference plot alone if these changes lead to a better estimate of ozone variability and trends, or not. Further discussion on the SAGE-composites is provided in Appendix A2.

3 Bayesian inference of the underlying ozone timeseries

We want to combine the information from the various composites and correctly account for uncertainties, artefacts and drifts. To this end, we adopt a Bayesian approach to infer constraints on the **(unknown)** true timeseries, $\mathbf{y}$, given the full set of data, $\mathbf{d}$. The data consists of n_c composites, indexed by c; each composite is made up of n_t measurements, indexed by t. A single measurement is hence $d_{t,c}$, where the index ordering is chosen to match that required for the matrix manipulations used in Section 3.1. The underlying timeseries that is to be inferred, $\mathbf{y}$, hence has individual elements y_t.

Bayesian inference necessarily involves conditioning on our knowledge about uncertainties and potential artefacts and drifts, and any prior assumptions about the month-to-month variability, through our model which we denote as M. Bayes's theorem allows us to combine this information in the form of the posterior distribution of the true timeseries given the data, model and any prior information $P(\mathbf{y}|\mathbf{d}, M)$:

$$P(\mathbf{y}|\mathbf{d}, M) = \frac{P(\mathbf{y}|M)\,P(\mathbf{d}|\mathbf{y})}{P(\mathbf{d}|M)}, \tag{1}$$

where $P(\mathbf{y}|M)$ encodes our prior information and assumptions about the month-to-month variability of the underlying true timeseries, the likelihood $P(\mathbf{d}|\mathbf{y})$ summarizes our probabilistic model for the data given the associated measurement uncertainties (including our knowledge and assumptions about the possibility of instrumental artefacts systematically biasing the observations at certain times), and the marginal likelihood $P(\mathbf{d}|M)$ in this situation just plays the role of a normalizing constant.

In order to form the desired posterior distribution we require a probabilistic model for the data (section 3.2) that incorporates our knowledge and assumptions about the observational uncertainties (section 3.1), and a clear statement of our prior assumptions (section 3.3). The resulting posterior density is a high-dimensional probability density over $\mathbf{y}$, where the length of the vector $\mathbf{y}$ (i.e., the number of time points in the timeseries) is typically of order $\sim 10^2$. Whilst direct evaluation of such high-dimensional probability densities on a grid is computationally unfeasible, they can be effectively reconstructed through sampling algorithms such as Markov Chain Monte Carlo (MCMC), discussed in section 4.

3.1 Uncertainty estimation

Our method requires uncertainties for each composite that reflect the actual differences between the reported values and the true state of ozone at the time of each measurement, as

encoded in the likelihood (Eq. 7). We cannot use the uncertainties published by the composite teams as they are (in general) not derived in the same way and so potentially encode information differently. The quoted uncertainties can include: (i) uncertainties propagated at each step of the data and composite processing, e.g., in regression analysis used to combine individual instruments; (ii) uncertainties in the absolute offsets; (iii) the total number of observations in each dataset; and (iv) precision and calibration errors. A natural choice might be to scale the uncertainty with the inverse square root of the number of observations used to form the monthly ozone value from each instrument, but this would not correctly deal with systematics such as, e.g., slow instrument drift (as experienced by the SBUV instruments during the 1995–2000 period). Using the number of data points to weight the monthly mean in each composite would lead to the most likely value simply following the SBUV data almost exclusively until 2005 (see Fig. A2 in the appendix), and drifts would remain in the final product (see section 4.3).

Instead, we seek to estimate the noise level from the data, and in particular from the discrepancies between the different composites. Estimating the uncertainties is not the main focus of this paper, so a simple heuristic method is used here, but this is clearly an aspect of this overall data analysis problem which should be investigated further. Our approach is based on a principal components analysis (PCA) of the composites to model the differences between them, with the time-dependent noise level of each composite then estimated from the variance of the higher order components. The starting point of this approach is to treat the full data-set $\mathbf{d}$ as an $n_t \times n_c$ matrix with elements $d_{t,c}$ as defined above. We then use this to construct the mean-subtracted data matrix $\mathbf{d}'$ with elements given by

$$d'_{t,c} = d_{t,c} - \frac{1}{n_t} \sum_{t'=1}^{n_t} d_{t',c}, \tag{2}$$

where each composite is treated separately. The PCA is implemented via singular value decomposition (SVD) in which the mean-subtracted data matrix is factorized as

$$\mathbf{d}' = \mathbf{U}\mathbf{W}\mathbf{V}^{\mathrm{T}}, \tag{3}$$

where $\mathbf{U}$ is an $n_t \times n_c$ matrix in which the columns are the orthogonal component timeseries, $\mathbf{W}$ is an $n_c \times n_c$ matrix giving the weights of the components, and $\mathbf{V}$ is an $n_c \times n_c$ matrix that encodes the contributions of the to components the composites. A standard PCA reconstruction of the (mean-subtracted) composites would then have the form

$$d'_{t,c} = \sum_{c'=1}^{n_c} U_{t,c'} W_{c',c'} V_{c',c}, \tag{4}$$

where the sum has to go from $c' = 1$ but is often truncated to include only the first few terms with the highest weights.

Our method of estimating the uncertainties in the composites is based on the above reconstruction formula, but is only heuristic in the sense that it does not follow from a rigorous calculation. We start by ignoring the leading, i.e., the highest weighted, mode in U as it is common to all composites, and so provides no extra information. The various noise artefacts are separated across the other $n_c - 1$ components, which must be combined somehow to reconstruct the noise. We make the natural choice to weight the modes by their respective contributions to each composite and then sum the resultant variances to obtain uncertainty estimates as

$$\sigma_{t,c}^2 = \sum_{c'=2}^{n_c} (U_{t,c'} \, W_{c',c'} \, V_{c',c})^2. \tag{5}$$

The steps of this method are illustrated in Figure 4. The left set of panels shows the SVD applied to ozone at 10 hPa 0–10°N: the SVD modes, **(i.e., from matrix U)** (black lines; first four panels) each have a different weight (percentage value in the lower right of each plot**, from matrix W**). The first mode contains most of the variance (84%) with the remainder split between the other three (13, 1 and 2%). The first mode is common to all four datasets, and its relative weight within each dataset is represented by the colored dots **(from matrix V)** to the right of each mode ranging from −1 to +1; the weight of mode-1 is similar in all four datasets. The second mode is split roughly equally between the two pairs of composites as indicated by the dots on the right, suggesting that it is the difference between the pairs, and for which the rescaled difference of SBUV-MER and GOZCARDS confirms, plotted in grey and with an almost identical variance to the SVD mode. The SBUV-composites have almost zero weight in the third mode, indicating that the mode represents artefacts only within the SAGE-composites, again confirmed by the difference between SWOOSH and GOZCARDS (grey). With almost zero weight for the SAGE-pair in the fourth mode, the rescaled difference between SBUV-pairs confirms the mode represents artefacts in SBUV.

From this, we form the uncertainty estimate for each of the composites in the bottom panel, $\sigma_{t,c}$. Unfortunately, the SVD can only be formed when there is data available in each composite, which leads to gaps, represented by the grey shading in the bottom panel. Because composite sub-periods have different uncertainty characteristics, we fill gaps using the median of the period between instrument changes in the composites (vertical lines in the four modes; colours relate to each composite).

In principle, the timeseries at each latitude-altitude location in the four composites should be the same, and any deviations from the true value should be a result of one or more of the potential reasons listed in section 4.3. By this assertion, the composites each contain the real timeseries and an additional set of artefacts. The problem is that we do not know for sure in which dataset a problem might be, especially if the true trend is only apparent in (or missing from) one composite, or one composite pair (i.e., SAGE- or SBUV-based). Thus, the SVD approach allows us to separate the common signal **(the leading mode in U corresponding to the highest weight in W**, from those that form the differences between the composites **(with lower weights)** and the real ozone. This leads to an attribution of higher uncertainty for single datasets that exhibit variance not present in

the other three, and allows us to assign higher uncertainties in all the composites when one pair (e.g., SAGE-pair) acts differently to the other pair (e.g., SBUV-pair). **In this way, it is a relatively conservative estimate.**

370   The example at 10 hPa was ideal since modes were easy to associate with artefacts within and between the composite-pairs. Another example of the usefulness of applying the SVD approach to estimate the uncertainty is shown for 2.2 hPa and 0–10°N in the right-hand panels of Fig. 4b. The first mode is ubiquitous to the composites, and the fourth mode shows a clear attribution to the SBUV-composites (the rescaled difference is shown in grey). However, it is not possible to attribute modes

375   two and three as confidently, though the artefacts are more likely from GOZCARDS and SWOOSH, respectively. Since complete separation of this mode from the other composites is not possible (e.g., that SWOOSH is definitely the reason for the third mode), some uncertainty is given to the other composites. This is an intuitive approach to assigning uncertainty to each of the composites.

    Satisfyingly, the error estimates display higher uncertainty to individual composites during periods

380   already known to have anomalous behavior (section 4.3). For example, in the lower panel of Fig. 4 at 2.2 hPa (right), GOZCARDS is assigned a particularly high uncertainty during the first five years, as expected (section 2.2.2). At 10 hPa (left), the SBUV composites generally have a higher assigned uncertainty, especially around mid-1995, and until 2000, when we know there are instrument drifts in the SBUV-composites (section 4.3). In summary, the SVDs allow us to independently and fairly

385   assign an uncertainty to each of the composites.

    As the SVD approach is not always able to assign a known artefact explicitly to a specific composite, it is necessary for us to provide additional information regarding the composite uncertainties, whereby in three cases we increase the estimated uncertainty by a factor of two. These are: (i) when an instrument changes in a composite, which is appropriate since there are many examples of jumps

390   in a composite on, or immediately after, these dates (e.g., Fig. 2c in 1994 and 1995); (ii) during known and significant instrument drifts in SBUV – the SBUV drift from the SVD uncertainty estimate is typically assigned equally to both pairs of composites and so additional information is needed and tests show that it is only partially accounted for when this additional information is not included – specifically 1995–2000 for both SBUV-composites, and additionally 1994–1995 in SBUV-MER

395   (these periods are marked by black shading and white text in Fig. 1); (iii) following the eruption of Mount Pinatubo in SBUV-MER only (see Fig. 1 and section 4.3).

3.2   The likelihood

With estimates of the uncertainties on each composite, we can construct the joint-likelihood function for the set of composites as a product over the individual likelihoods at each time-step (indicated by

400   t) and composite (indicated by c), so that

$$P(\mathbf{d}|\mathbf{y}) = \prod_t \prod_c P(d_{t,c}|y_t), \tag{6}$$
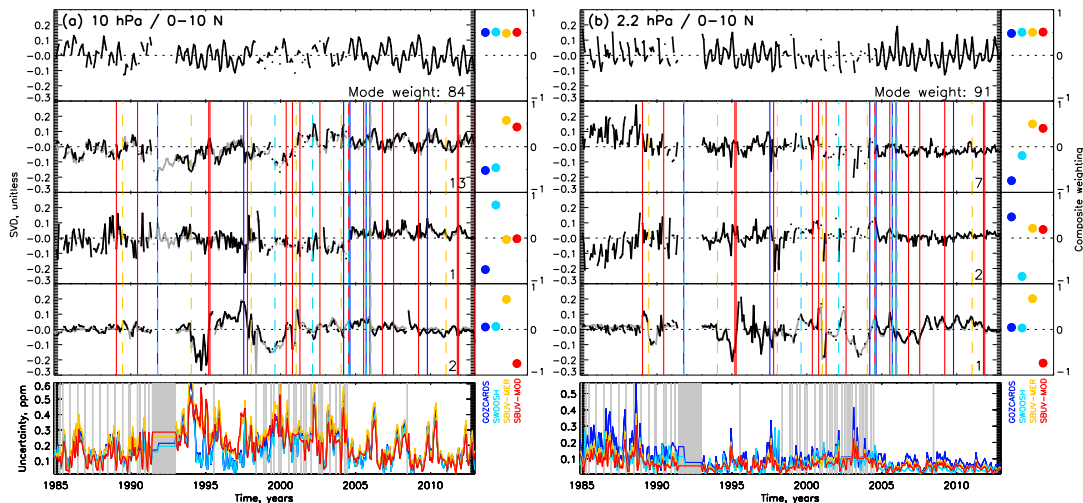
Figure 4: Visualisation of the components of the SVD algorithm within the BASIC approach used to estimate the uncertainty on each ozone composite for two examples at (**a**) 10 hPa and (**b**) 2.2 hPa at 0–10°N. The left column of the first four rows show the determined singular value decomposition (SVD) unitless modes (black time series); the mode weighting (%) is given in the bottom-right; the right column is the mode weighting for each composite. All colours represent information related to GOZCARDS (blue), SWOOSH (light-blue), SBUV-MER (yellow) and SBUV-MOD (red). Vertical lines represent dates an instrument change in the composite occurred. The grey timeseries is the arbitrarily rescaled difference between SBUV-MER–GOZCARDS, SWOOSH–GOZCARDS and SBUV-MER–SBUV-MOD in (a) in rows 2–4, and SBUV-MER–SBUV-MOD in (b) in row 4. The bottom panel (row 5) in (a) and (b) represents the uncertainty derived from the root sum of the squares of the modes (rows) 2–4, weighted by the mode and composite weight, in units of ppm. Grey vertical lines represent dates when data in any composite is missing and filled with the median uncertainty for the sub-period in which they lie (i.e. between the vertical lines in rows 2–4).

which implicitly assumes that the measurement errors at different time-steps and between different composites are uncorrelated.

A common assumption would be that, ordinarily, the likelihood for a single measurement would
405 be taken to be a normal distribution with a mean given by the true value, y_t, and a standard deviation of $\sigma_{t,c}$, the measurement uncertainty in composite c at this time-step. However, it is clear from even a quick inspection of the data that there are significant disagreements between the different composites, implying several of them – and possible all – are far more prone to extreme errors (i.e., outliers) than would be predicted by a simple Gaussian likelihood. We hence adopt the model of Box
410 and Tiao (Box and Tiao, 1968) in which there is a probability $0 \le \beta \le 1$ that any given measurement

has an uncertainty inflated by a factor of $\gamma \geq 1$, such that the likelihood for a single measurement is

$$P(d_{t,c}|y_t) = \frac{1}{\sqrt{2\pi}\,\sigma_{t,c}} \left\{ \frac{\beta}{\gamma} \exp\left[-\frac{(d_{t,c} - y_t)^2}{2\gamma^2 \sigma_{t,c}^2} \right] + (1 - \beta) \exp\left[-\frac{(d_{t,c} - y_t)^2}{2\sigma_{t,c}^2} \right] \right\}. \tag{7}$$

Smaller values of β encode more faith that uncertainties, $\sigma_{t,c}$, are correct; higher values of γ correspond to more catastrophic outliers. The standard normal distribution is recovered if either $\beta = 0$ or $\gamma = 1$. Both β and γ must either be fixed by hand or kept as hyper-parameters to be inferred. We fix $\beta = 0.1$ and $\gamma = 100$, which implies that we consider outliers reasonably rare, but extreme should they occur; this choice leads to multi-modal behavior as desired (see section A3 and Fig. A3).

When the multiple measurements of the different composites are combined in the product over c, the resultant likelihood can be multi-modal when considered as function of y_t. In cases where the composites disagree the implication is that it is most likely that one of the measurements is good, but not necessarily which is to be preferred. By contrast, simply multiplying Gaussian likelihoods together in such a situation would result in a joint likelihood that sits between the two (or more) peaks and does not represent likely values according to any of the composites **(left column of Fig A3)**. However, under the model prescribed by Equation 7, the joint likelihood is multimodal where subsequent application of the prior may elicit which of the peaks is representative of the truth and which observations were likely dominated by artefacts (or indeed if all composited might be systematically biased simultaneously but in different ways, in which case the resulting posterior for that point will have an inflated uncertainty as desired).

3.3 Transition prior

We factorize the prior into a product of transition priors for each month-to-month transition, i.e.,

$$P(\mathbf{y}) = P(y_0) \prod_{t=1}^{N-1} P(y_{t+1}|y_t). \tag{8}$$

The transition prior provides a way to estimate if measurements of ozone values from the composites in the month being evaluated are more likely or not, and hence provide a way of assessing anomalous behavior. The annual, or semi-annual, variability that makes up the seasonal cycle, is the largest mode of ozone variability. It is also a relatively consistent mode, so together with information from the observations, it can provide a way to help differentiate between artefacts and real anomalous behavior.

We form the transition prior from all four composites together. Two examples are given in Fig. 5 at 2.2 and 10 hPa at 0–10°, where the expected change between month n and n+1 for the whole year is shown, with e.g. $n = 1$ being the transition between January and February. The monthly changes for all composites are shown with the box-and-whisker plots, which show the mean (white horizontal line), inter-quartile range (IQR, 25–75th percentiles; thick stem) and full range or 1.5 times the

IQR (thin line), with any outliers given as dots; **data in a composite where instruments change is not included in the estimates**. The grey Gaussian distributions are formed from all the changes between two months treated independently and then performing 1000 bootstraps. We note that in the examples shown in Fig. 5, the SAGE-based composites typically have a larger range of month-to-month variance, which we suggest may be due to the higher resolution of the SAGE-composite instruments, but we cannot exclude the possibility that this is also related to the low-sampling and higher scatter of, e.g., the earlier observations from SAGE-II.

4   Posterior sampling

With the likelihood (section 3.2) and prior in hand, we can construct the posterior density for the true timeseries given the data and our prior knowledge and assumptions, ie., equation (1). The product of the prior (Eq. 8) and the likelihood (Eq. 7) over all the observations gives the numerator of the posterior density defined in Eq. 1. The normalising denominator cannot be calculated analytically, but fortunately the numerator is sufficient to obtain samples from the posterior distribution. We sample the posterior using Hamiltonian Monte Carlo (HMC) sampling (Neal, 1993) implemented in STAN[1] (Carpenter et al., 2016), which is particularly effective at sampling high-dimensional densities (Neal, 1993). The resulting inferred ozone timeseries forms the BASIC composite.

4.1   BASIC approach as an approximation to a Bayesian hierarchical state-space model

When constructing the month-to-month transition prior as described above, we use the data to estimate and fix the prior's hyper-parameters, ie., the means and variances of each month-to-month transition (Jan-Feb, Feb-Mar etc). This is using the data twice – once to construct the transition prior, and once in the main posterior inference. However, we note that estimating and fixing the hyper-parameters from the data is an approximation, similar to 'empirical Bayes' methods, to a full Bayesian hierarchical treatment where the parameters of the prior would be kept as free unknown parameters and inferred jointly with the true ozone timeseries. In cases where the hyper-parameters are tightly constrained by the data and do not strongly co-vary with the parameters of interest (here, the underlying ozone timeseries), estimating and fixing the hyper-parameters from the data before the main analysis is an excellent approximation to the full hierarchical model. [2]

---

[1] STAN software can be found at http://mc-stan.org

[2] **We leave a more careful hierarchical analysis to future work, expecting this approximation to have a small impact on the results, but outline the full hierarchical model briefly below for completeness. In the generative hierarchical**
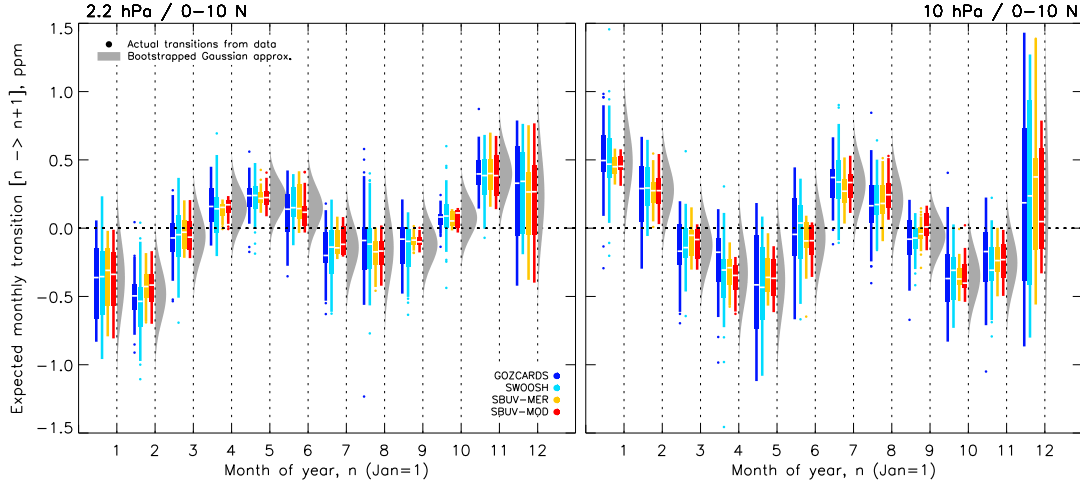
Figure 5: The expected monthly ozone changes (or 'transitions') between month n and the next month, n+1, i.e. index 1 represents a change between January and February. We show two examples at 0–10°N: (left) 2.2 and (right) 10 hPa. The box-and-whisker plots are for all observations when no change in the underlying instrument of the composites occurred and represent the inter-quartile range (IQR) covering the 25th to 75th percentiles (box) and 1.5 times the IQR or the maximum, whichever is smallest (whisker); outliers are plotted as dots. Plotted to the left of the vertical lines at each index are the changes between months for each composite (represented by the different colours); Gaussian distributions to the right of the vertical lines represent those formed from the mean and standard deviation of all the composite transitions from 1000 bootstraps. These Gaussians are used as transition-prior estimates and are calculated for all pressures and latitudes.

---

model, the true ozone timeseries are generated from the transition prior as

$$y_t = y_{t-1} + \Delta_t$$

$$\Delta_t \sim \mathcal{N}[\mu_{m(t)}, \sigma_{m(t)}],$$

where the mean μ_m and variance σ_m depend only on the month of the year, $m(t)$, corresponding to the time-step t, and broadly capture the stochastic month-to-month variability as described above. The individual composite datasets are then generated from the Gaussian-mixture model described in Equation 7 as

$$d_{t,c} \sim (1-\beta)\mathcal{N}(y_{t,c}, \sigma_{t,c}^2) + \beta\mathcal{N}(y_{t,c}, \gamma^2\sigma_{t,c}^2)$$

where β and γ describe the outlier rate and outlier uncertainty inflation-factor, respectively, and $\sigma_{t,c}$ is the assumed measurement uncertainty. Since in general we do not know the hyper-parameters of the prior (μ_m and σ_m) or the Gaussian-mixture nuisance parameters (β and γ) a priori, the most principled Bayesian solution is to infer the joint posterior distribution for the true ozone timeseries y and the hyper- and nuisance- parameters together, and formally marginalize over the latter. We leave this full treatment to future work and here estimate and fix the prior hyper-parameters, and choose the Gaussian-mixture parameters heuristically.

4.2 Example results of the BASIC approach

We designed tests to evaluate whether the BASIC approach was effective in retrieving the 'true'
ozone timeseries given a set of four ozone composites that had jumps, drifts and noise, similar to
those we encounter in the existing datasets. Overall, we found the BASIC approach to be successful
at estimating ozone and, in particular, better than any individual composite that contains artefacts.
These tests are presented in Appendix A5.1.

The BASIC composite result for the 0–10°N 2.2 hPa timeseries is given in Fig. 6a, with all four
composites, and the BASIC composite with uncertainties at two-standard deviations (dotted lines)
and 68, 95 and 99% **credible intervals** (dark, medium and light grey shading); the differences in
Fig. 6a relative to the BASIC composite are shown in Fig. 6b. It is clear that the BASIC approach
has successfully accounted for (i) the early drift prior to 1991 in GOZCARDS resulting from the
use of NCEP reanalysis temperatures, and (ii) the high scatter in both the SAGE-composites prior
to 1991 and mainly in SWOOSH prior to 2004 resulting from the low-sampling of the occulta-
tion instruments used. When disagreement between composites increases, or the priors inflate the
uncertainties, the BASIC composite uncertainty estimate naturally inflates to allow for the higher
uncertainty during that period; on the other hand, the BASIC composite uncertainties reject most of
GOZCARDS prior to 1989 **by being outside the 99% credible interval**.

Another example, at the higher pressure of 10 hPa, is given in Figs. 6c and d. Here we see that
the BASIC approach has accounted for (i) the SBUV-MER problem following the Mt. Pinatubo
eruption, during which SBUV-MOD measurements are not provided, (ii) rapid steps in the SBUV-
composites between 1995 and 2001, and (iii) some of the drifts in the SBUV-composites during the
same period. What is clear here, especially in the period after 2002, is that while the BASIC com-
posite reproduces most of the variance, it cannot determine whether the higher amplitude variance
of the QBO signal in the SAGE-composites is more likely to be correct than the SBUV-composites,
though we know the reason is due to the lower vertical resolution of the SBUV-type instruments and
that the QBO represented by the SAGE-composites is more likely to be correct (see section 4.3).
We do not currently have a solution for this particular issue, though the errors do inflate naturally to
accommodate this uncertainty, and so **typically** within the uncertainties this issue is captured by the
BASIC approach.

Finally, to show how the BASIC approach operates in a completely different regime to that near
the equator, in Fig. 6e and f we give an example at 6.8 hPa and 50–40°S. Here, ozone lacks a
semi-annual component of variability. Except for between 1993 and 2001, all four composites show
broadly similar variability. The SAGE-composites again appear to show spikes that aren't present
in the SBUV-composites, and indeed on many occasions do not occur in both SAGE-composites.
Therefore, many of these are rejected by the BASIC composite. We cannot discount that some of
these artefacts are a result of the better resolution in the SAGE-composites and may be real, for
example unexplained artefacts after 2008, but these are generally found to remain at or **within the**
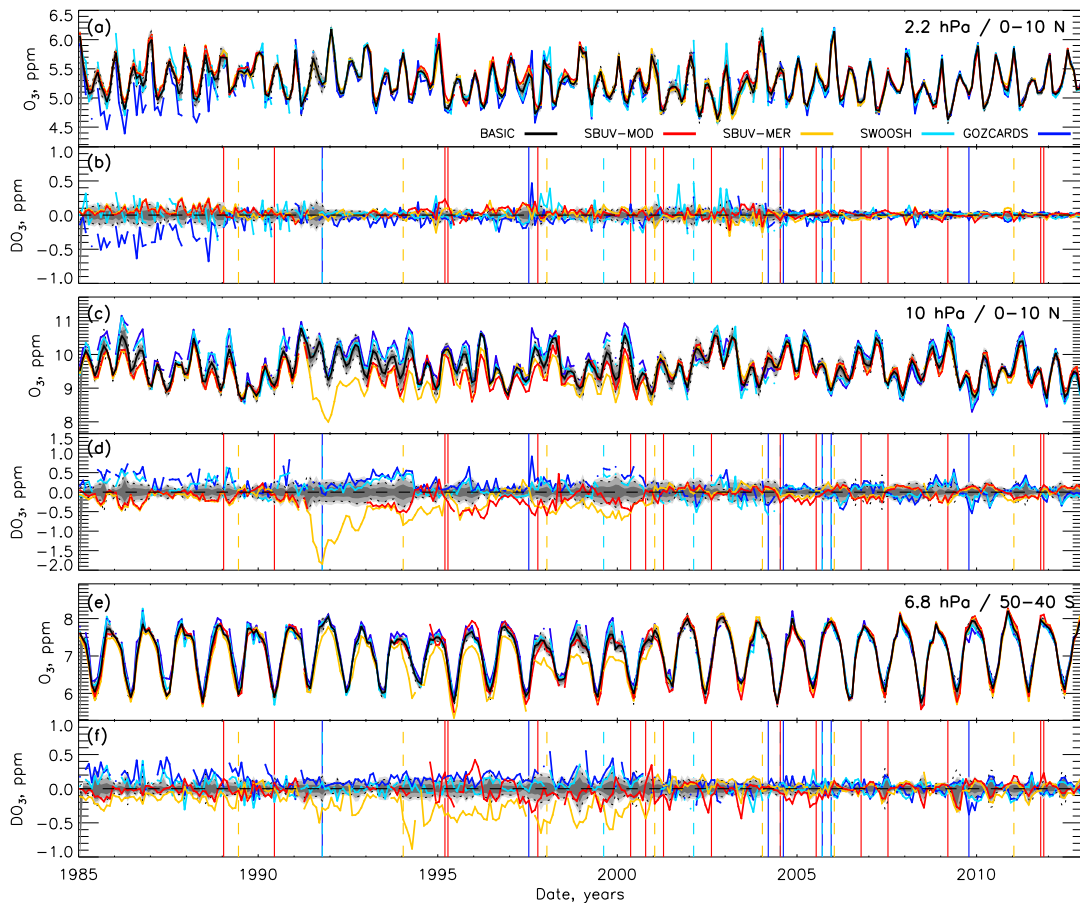
Figure 6: Ozone time series at three stratospheric locations from 1985–2012, all bias-shifted to the mean of SWOOSH after August 2005. (**a**) Absolute ozone at 2.2 hPa over 0–10°N from SWOOSH (light-blue), GOZCARDS (blue), SBUV-MER (yellow), and SBUV-MOD (red). The BASIC composite mean estimation (black) is plotted with shading representing 68% (dark-grey), 95% (grey) and 99% (light grey) credible intervals (CIs); these CIs are not Gaussian, so 2 times the standard deviation is also plotted with thin dotted lines. (**b**) As for (a), but now the difference relative to the BASIC composite. (**c**) and (**d**) are as for (a) and (b) at 10 hPa and 0–10°N, and (**e**) and (**f**) are as for (a) and (b) at 6.8 hPa and 50–40°S. Vertical dashed and solid lines in (b), (d) and (f) identify changes in the instruments used in the composites.

510 **99% credible interval**. Following the instrument change in SBUV-MER in 1994, and until 2001, we see anomalous behaviour in SBUV-MER that is **rejected by the BASIC composite at the 99% level** throughout this period; between 1995 and 1997, SBUV-MOD also displays behaviour quite different to the other composites, and this is also generally rejected.
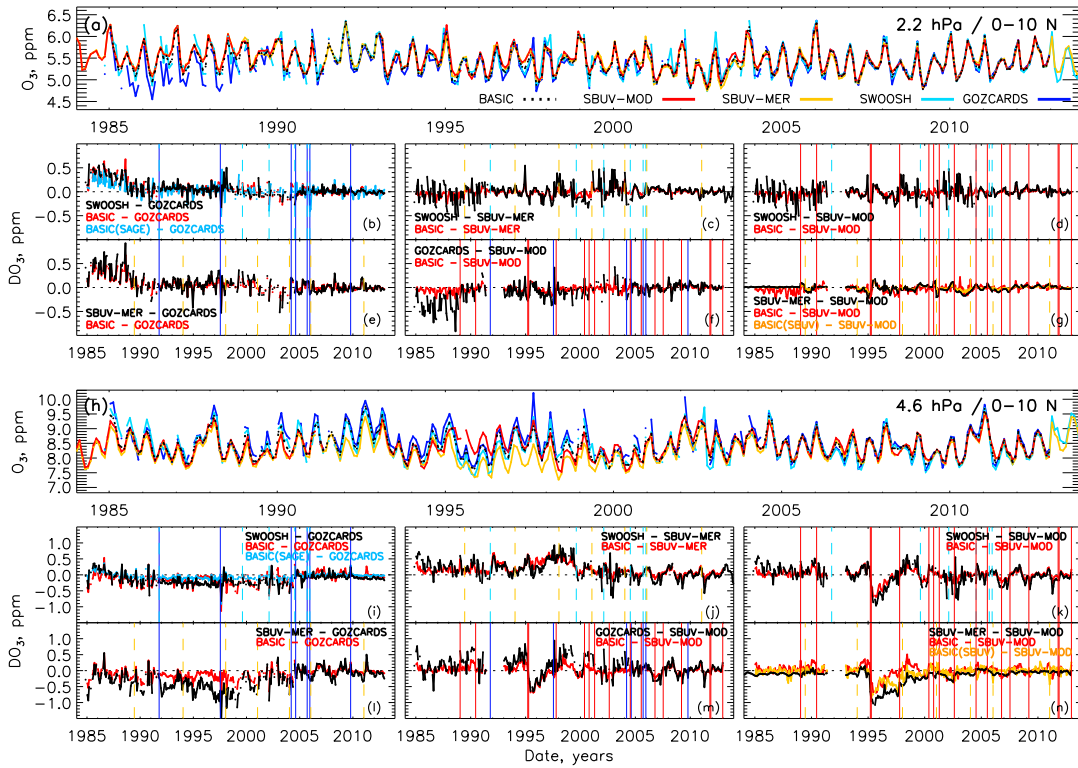
Figure 7: Ozone time series at two stratospheric locations from 1984–2014, all bias-shifted to the mean of SWOOSH after June 2005. (**a**) Absolute ozone at 2.2 hPa over 0–10°N from SWOOSH (purple), GOZCARDS (blue), SBUV-MER (yellow), and SBUV-MOD (red). (**b-g**) The difference between each pairing of the four composites and with the BASIC composite (see legends). (**h–n**) As for (a–g) but at 4.6 hPa and 0–10°N. Solid and dashed vertical lines represent months with a change in the instrument used to construct the composite (colours are with respect to the composite colour in (a) and (h).

4.3 Further examples of problems resolved by the BASIC approach

515 In sections 2.2.1 and 2.2.2, we showed examples of differences between composites based upon the same, or similar, instrument data. It is not always clear by looking at the pairs of composites, however, which is more likely to be correct: drifts and rapid changes occurring over a few months cannot be immediately attributed to a specific composite. However, as we will now demonstrate, additional information from the literature, knowledge of when instruments are added or removed within the 520 composites, and looking at the differences of all four composites at the same time, helps to build confidence in attributing the source and reason for the deviation, and then correcting it – these are encoded in the uncertainties of each composite as discussed in section 3.1. We also show the effectiveness of the BASIC approach in accounting for most of these artefacts. The final BASIC ozone

composite product that integrates information from all four composites is denoted 'BASIC'. But, it

525 is also possible to only use information from either the SBUV-pair ('BASIC(SBUV)') or SAGE-pair ('BASIC(SAGE)') of composites (with SVD uncertainties and transition priors constructed using only the respective pairs of data), which elucidates how the prior information applied in the BASIC algorithm is able to perform if information is missing from the other pair of composites. In other words, a correction of artefacts (e.g. drifts in SBUV-composites) that do not appear in differences of

530 just one composite pair strengthens our claim that the BASIC approach is correctly accounting for artefacts in the composites. For clarity in the figures introduced here, we do not provide uncertainties on the BASIC results presented.

In Fig. 7 we show two examples of the four ozone composites at 0–10°N, at 2.2 hPa (a–g) and 4.6 hPa (h–n). Below the absolute timeseries (a and h) are six plots (b–g and i–n), which are the

535 differences between each pairing of composites (black); the absolute BASIC composite ozone is shown with a dotted line, and differences of the BASIC, BASIC(SAGE) and BASIC(SBUV) compared to the composites are given in red, blue and orange, respectively. Once again, the early drift (e.g. (b) SWOOSH – GOZCARDS) and the steps (e.g. (n) SBUV-MER – SBUV-MOD) are clearer in these restricted latitude bands than in the broader equatorial band presented in Figs. 2c and 3c.

540 However, considering these different pressures and latitudes, and the SBUV–SAGE differences (c–f), additional anomalous behaviour is revealed, which we list and discuss in the following.

1. The most significant problem in creating a unified calibration for all SBUV instruments is the orbital drift (McPeters et al., 2013). Ideally, the local time at equator crossings should be the same each orbit, and the orbit should be near-polar to attain near-global coverage. However,

545 NOAA satellites slowly drifted over time, changing from near 2pm (10am, NOAA-17) equator crossings to late afternoon (early-morning, NOAA-17) equator crossings. NOAAs 9, 11, 14 and 16 drifted through the terminator and began making early morning measurements. The equator-crossing time for each of the SBUV satellites is shown in Fig. 1 between the SBUV-MOD and -MER composite information. Any instrument or calibration errors may be signif-

550 icantly enhanced for observations taken as the orbit approaches the terminator, such that the orbit drift can lead to an apparent time-dependent trend in ozone that could be misinterpreted as real; McPeters et al. (2013), DeLand et al. (2012) and Bhartia et al. (2013) do not recommend the use of near-terminator data for this reason. Accordingly, SBUV-MOD, with the exception of NOAA-11, does not include any observations taken outside the 8am–4pm equato-

555 rial crossing time range (marked as dotted horizontal lines in Fig. 1) and similarly SBUV-MER prioritizes measurements made while instruments are in their optimum orbits. The clearest example of this drift-related trend can be seen in Fig. 7k, m and n in all differences with respect to SBUV-MOD between 1995 and 1998 (until 2000 with respect to SBUV-MER in Fig. 7n); there is then a reversed drift until after 2000. The differences with the SAGE-composites in-

560 dicate that: a 1994–1995 drift is likely in SBUV-MER from the exclusive use of NOAA-9;

for 1995–1997 the drift is probably in both, but more prominent in SBUV-MER differences; the 1997–2000/2001 drift is more likely in SBUV-MER with the exclusive use of NOAA–11 (SBUV-MOD merges NOAA-11 with NOAA–14). Other, smaller drifts between the SBUV composites are visible in (n), e.g. in 2001 and 2002. While BASIC(SBUV) and BASIC were

565   able to account for the large discontinuity present in Fig. 7n, BASIC(SBUV) is unable to account for the 1997–2000 drift in SBUV-MOD. We do inform the BASIC approach that the uncertainties should be increased in the SBUV-composites during the drift period 1995–2000 (from 1994 in SBUV-MER), so uncertainties are equal for this period in BASIC(SBUV). Nevertheless, with the inclusion of the SAGE-composites this drift can be accounted for (red line

570   in Fig. 7j–n), which further reinforces the need for information from all composites to resolve problems. Confirmation of drift problems during the periods mentioned (DeLand et al., 2012; McPeters et al., 2013; Kramarova et al., 2013b; Frith et al., 2014) justifies using it as prior information to down-weight these data for this time (see Appendix A1 for more information).

2. The apparent high scatter at 2.2 hPa in all differences involving SAGE-composites (i.e Figs. 7b–

575   f) during the periods of 1985–1991 and 1997–2004 coincides with periods when only occultation instruments were active (SAGE-II, UARS/HALOE and ACE-FTS). Toohey et al. (2013) and Sofieva et al. (2014) convincingly demonstrated that insufficient and/or inhomogeneous sampling can result in inaccurate monthly estimates and even induce spurious spikes in ozone timeseries; coarse-sampling occultation-type instruments such as GOMOS and ACE-

580   FTS, can lead to differences of up to 20%. This can especially affect seasonal cycle representation, especially at high altitudes where ozone undergoes rapid variations with latitude and time of day. This is why spurious variability from occultation instruments is clearly evident in Fig. 7 during the aforementioned periods. Even though satellite measurements from limb-viewers have a lower vertical-resolution than occultation, these are still sufficient to reduce

585   the monthly zonal-mean scatter in the SAGE-based composites when overlaps with occultation instruments occur (e.g. 1992–1997 in GOZCARDS). The BASIC–GOZCARDS difference in Fig. 7e agrees closely with the month-to-month artefacts that are highlighted in the SBUV-MER–GOZCARDS difference. This is not because of the information provided in the SBUV-composites, which don't display this behaviour, but because the deviation from the nat-

590   ural seasonal cycle is so high that the month-to-month seasonal variability is more informative. This is confirmed by the high agreement between BASIC–GOZCARDS with BASIC(SAGE)–GOZCARDS on these short-timescales in Fig. 7b, the latter of which contains no knowledge from the SBUV-composites.

3. The drift between the SAGE-composites prior to 1991 (Figs. 7b and i; see section 2.2.2) is

595   largely absent in the SWOOSH composite compared to SBUV-composites (Figs. 7c and d), confirming it as a feature of GOZCARDS only. It is clear from Fig. 7e that the artificial

trend in GOZCARDS prior to 1991 is fully accounted for by BASIC, and once again the agreement of BASIC–GOZCARDS with BASIC(SAGE)–GOZCARDS in Fig. 7b shows that the information in the SAGE-composites alone is sufficient to eliminate most, though not all, of this problem. No prior information about the drift being in GOZCARDS is provided to the BASIC approach – the ability for the BASIC approach to account for the drift is most likely because SWOOSH agrees with the prior information from the seasonal variability (in the transition prior) much better than GOZCARDS.

4. A small downward step in the SAGE-composite difference in Fig. 7b and i in 2004 occurs around the time both SAGE-composites have an instrument change. This feature is more evident in the differences between GOZCARDS and the SBUV-composites than for SWOOSH, at both altitudes. At the lower altitude of 4.6 hPa in Fig. 7i, it appears that BASIC(SAGE) could not account for the jump in GOZCARDS, and ends up slightly offset from the black difference line. The BASIC approach performs better with the additional information provided by the SBUV-composites, and fully accounts for this jump.

5. A prominent feature in Fig. 7j–m is the approximately 2–3 year oscillation. This is the result of lower vertical resolution in the SBUV observations, which leads to a damping of the quasi-biennial oscillation (QBO) signal in SBUV relative to the higher resolution instruments of the SAGE-based composites; at 3 hPa SBUV has a vertical resolution of approximately 6-7 km, while the SAGE-based instruments are usually better than 3.5 km - the vertical resolution only gets larger for SBUV with lower altitude, reaching a maximum of ~15 km below the tropopause (Bhartia et al., 2013). After 2003, the resolution effect is more clearly visible in Fig. 7h, since many of the other instrument-data/composite artefacts are absent. Kramarova et al. (2013a) showed that by applying the SBUV resolution kernel to higher vertical-resolution Aura/MLS data led to good agreement with SBUV data. Focusing on the period after 2005 in Figs. 7h–n, it is evident that the BASIC is unable to distinguish between the QBO represented in the SAGE- and SBUV-composites; this is because uncertainties are similar during this period and composite issues are generally absent. We discuss this further in Appendix A5.2.

6. Following the eruption of Mt. Pinatubo in June 1991, there is a large drop in SBUV-MER at 10 and 16 hPa due to interference in viewing from volcanic aerosols (not shown here, but see Fig. 6c and d), which is absent in the SAGE-composites; SBUV-MOD does not include data during this period. Ozone is usually depleted by sulphate aerosols following a volcanic eruption, but at lower altitudes. Due to the rapid departure of SBUV-MER from the SAGE-composites, the BASIC composite predicts that the SAGE-composites are more likely to be correct during this period. To be clear, the BASIC approach can adapt to rapid, unexpected changes in ozone: if all the datasets had shown a sudden, and similarly large change that was significantly different from the prior expectation for that month, it would tend towards a tighter

cluster of observations as more likely than the broader prior estimate. We discuss this period further in appendix A5.2.

635 7. For completeness, steps in the SBUV-composites in Figs. 7k, m and n, discussed in section 2.2.1 occur in 1995, and in 2003, 2004 and 2007 in n; though these are not the only times that steps occur; prominence of steps depends on altitude and latitude. The BASIC approach accounts for these discontinuities, which is most clear for the large jump in the SBUV–MOD composite in Figs. 7k, m and n; absence of a jump in Fig. 7i confirms the success of the BASIC

640   approach. For the BASIC(SBUV)–SBUV-MOD case in Fig. 7n (orange), which relies exclusively on the SBUV-composites, the large step in 1994/1995, and drift that follows, is mostly accounted for.

5 Results

Now that we have established the validity of the BASIC approach, and constructed an ozone compos-
645 ite from GOZCARDS, SWOOSH, SBUV-MOD and SBUV-MER, we turn to analysing trends and modes of variability. This is often performed using multiple linear regression (MLR) (WMO/UNEP, 1994; Soukharev and Hood, 2006; Chiodo et al., 2014; Kuchar et al., 2015; Harris et al., 2015). However, the use of Dynamical Linear Modelling (DLM), first applied to ozone data by Laine et al. (2014), appears to be more robust at estimating the background trend, especially if it is non-linear.
650 Laine et al. (2014) noted this when comparing their DLM results with the MLR results of Kyrölä et al. (2013) where linear trends were sometimes found to be inverse to those estimated using DLM. We performed tests upon the artificial timeseries used to evaluate the performance of both methods with the BASIC approach (section 4.2 and appendix A5.1). We briefly introduce both methods below. We compare their performance on the artificial timeseries and the BASIC correction, introduced
655 in Appendix section A5.1, in Appendix section A6. We found that in every test-case the DLM did equally well, or better, at estimating the true background 'trend' than the linear estimate from MLR (see appendix Figs. A9 and A10), both for non-linear background trends and for timeseries with large artefacts.

5.1 Multiple linear regression (MLR) analysis

660 We perform MLR analysis on deseasonalised timeseries (i.e. by subtracting monthly means) using five regressors: the F30 radio flux (solar), which is superior to the F10.7cm radio flux for representing solar UV variability (Dudok de Wit et al., 2014); the stratospheric aerosol optical depth (SAOD (Sato et al., 1993), for volcanic eruptions); the El Nino Southern Oscillation (ENSO); and two orthogonal modes of the dynamical quasi-biennial oscillation (QBO). These regressors are displayed
665 in the upper part of Fig. 1. When we analyse decadal trends between 1985–1997 and 1998–2012, we use a linear trend to estimate the long-term trend. We use pre-whitening and a first-order autore-

gressive process (AR1) to account for auto-correlation in the residuals (Tiao et al., 1990). Statistical significance of the regression coefficients was evaluated with a Student's t-test.

5.2 Dynamical linear modeling (DLM)

670   We perform a dynamic linear modeling (DLM) analysis following very closely the model and formalism of Laine et al. (2014). We use the same five regression components as in the MLR. We allow for two modes of seasonal variability in the fit (with 6- and 12-month periods), where additional (Gaussian-process) variability of the sinusoidal seasonal modes is also allowed for (following Laine et al. (2014)), and variance of the (Gaussian) seasonal model-variability σ_{seas}^2 is kept as a free pa-

675   rameter in the fit. We include an AR1 process, where the variance σ_{AR}^2 and correlation coefficient ρ_{AR} of the AR process are also kept as free parameters in the fitting process. In contrast to MLR, the DLM approach allows for a fully non-linear 'trend', where the degree of non-linearity σ_{trend} is also kept as a free parameter in the fit (see Laine et al. (2014) for details). In further contrast to MLR, the Bayesian DLM approach jointly fits for the non-linear time-varying trend, the regression coefficients

680   of the five proxies and seasonal modes, as well as the nuisance parameters σ_{seas}, σ_{AR}, ρ_{AR}, σ_{trend}; uncertainties in the nuisance parameters and regression coefficients are formally marginalized over when stating inference of the trend, leading to a principled propagation of uncertainties. Similarly, uncertainties in the nuisance parameters and trend can be marginalized over when we are interested in the regression coefficients.

685   Our DLM analysis follows Laine et al. (2014) except for some small differences in the prior choices. For σ_{trend} we use a positive half-Gaussian prior with zero mean and dispersion 0.0005. For σ_{seas} and σ_{AR} we take positive uniform priors over $[0, \infty]$, and for the correlation coefficient of the AR process we take a uniform prior over $[0, 1]$, assuming that negative correlations are unphysical in this context. We also do not impose an external prior on the initial value of the AR process, as is done

690   in Laine et al. (2014), but draw the initial value of the AR process from its stationary distribution, ie., $\mathcal{N}(0, \sigma_{\text{AR}}/\sqrt{(1-\rho_{\text{AR}}^2)})$. Recovery of the DLM parameters $\{\sigma_{\text{trend}}, \sigma_{\text{seas}}, \sigma_{\text{AR}}, \rho_{\text{AR}}\}$ under the chosen priors is shown in a set of figures in Appendix A4.

5.3 Multi-decadal changes in ozone

Here, we present estimates of changes in ozone between 1985 and 1997, and between 1998 and

695   2012 (Fig. 8). This is the first time that DLM has been applied to these composite datasets, including recently updated SWOOSH and SBUV-MER. While we focus on the DLM results, we also refer to results using MLR given in appendix Fig. A11.

  Typically, ozone trends are reported as linear decadal percentage changes in three latitude bands in the Southern hemisphere (60°–35°S), over the equator (20°N–20°S), and in the Northern hemisphere

700   (35°–60°N) with sub-periods ending and starting in December 1997 and January 1998, respectively, as shown in Fig. 8 (appendix Fig. A11 for MLR) (WMO, 2014; Tummon et al., 2015; Harris et al.,

2015). These integrated latitude bands were formed by averaging the area/latitude-weighted 10°, with the 30–40° band receiving half the weight of the equivalent full band; the resultant timeseries were then analysed.

705   It does not make sense to provide a linear trend estimate for the non-linear DLM background trend. Instead, in Fig. 8 we give the percentage change of ozone between the first and last months of the sub-periods, i.e., between January 1985 and December 1997 (top row) and January 1998 and December 2012 (lower panels). Uncertainties represent the 95% credible intervals of the change for all 100,000 samples estimated with the DLM algorithm (shading for BASIC, bars for all others).
710 Since we do not show decadal trends for the DLM (but do for MLR in the Appendix), we also show as dashed black lines in Fig. 8 the mean MLR-BASIC linear trend profiles from Appendix Fig. A11, scaled from decadal changes to the longer, 13- and 15-year, sub-periods.

      In the earlier, 1985–1997, period the DLM and MLR profiles agree well (within the DLM uncertainty). The DLM-BASIC typically displays better agreement with the GOZCARDS profiles than the
715 others in the northern and southern mid-latitudes, but the mean profile is generally closer to that of SBUV-MOD over the equator. Indeed, above 4 hPa, SWOOSH is typically at or outside the BASIC composite 95% credible interval in northern and equatorial bands (this is also the case with MLR). Interestingly, the SBUV-composites are often outside the MLR-BASIC uncertainty range above 7 hPa at mid-latitudes in both hemispheres; DLM uncertainties are larger and the four composites in
720 closer agreement when trends are analysed using DLM. This might hint that MLR is being biased by residual variance and/or underestimating error bars, in contrast to DLM, as was observed in the test cases (see section A6). Overall, the 1985–1997 DLM results are consistent with previous studies and MLR, with a significant decline in ozone above 7 hPa at all latitudes, especially at mid-latitudes, and negative but usually insignificant trend at lower altitudes.

725   The results for the latter period, 1998–2012, show a significant positive trend in the upper stratosphere above 7 hPa, as expected to occur following the implementation of the Montreal Protocol. The result is significant in every dataset analysed with DLM in both the northern and southern mid-latitudes at at least one pressure level; for the BASIC composite the result is clear at multiple altitudes. We note that the MLR results are only statistically significant at northern mid-latitudes
730 for both SBUV-composites, and for all composites in the southern mid-latitudes at 3.2 and 4.6 hPa. There are also statistically significant differences between the mean MLR-BASIC and the DLM-BASIC profiles over the equator and at northern mid-latitudes; in the southern region DLM profiles for composites are less consistent than when using MLR, but the DLM-BASIC results are in good agreement. The DLM profile shapes in the northern hemisphere are consistent with each other, with
735 a negative trend in the lower stratosphere, though usually insignificant at the 95% level, and a positive response in the upper stratosphere, confirming the result of Harris et al. (2015). Interestingly, with the exception of SBUV-MOD, the large and significant negative MLR trends seen in **most of** composites at 7 hPa disappears when using DLM, except in GOZCARDS. This anomaly was found

in an integrated-set of seven composites by Harris et al. (2015), though not in the multi-model mean of the same composites in Tummon et al. (2015). These results suggest that it may be an artefact of the analysis approach rather than a real feature and further investigation is required.

In Fig. 9, we plot the DLM moving-trends as a percentage change in ozone relative to 1998; only the BASIC composite uncertainty is presented[3], and the MLR-BASIC linear trends pre-1998 and post-1997 are given as dashed lines; as a guide the MLR uncertainties are typically smaller than the DLM (see Fig. A11). From Fig. 9, significant disagreement at 5–10 hPa at the equator and **15–22 hPa** in the southern hemisphere is very much apparent at the altitudes where DLM and MLR trend estimates disagree on the sign of the trend; this instability of MLR was also noted by Laine et al. (2014) and requires investigation in a future publication to understand. Fig. 9 also allows us to observe how the background evolves with time; from this we can see that, while SBUV-MER often displays large deviations from the group (e.g. especially at 5 and 7 hPa in all latitude bands), the BASIC composite results are almost always smoothly varying and generally monotonic to/from the years 1998–2002, meaning that a comparison between MLR trends and a change between fixed dates from the DLM is indeed valid (the exception possibly being at 2, 1.5 and 1 hPa over the equator where all datasets display relatively rapid variations in the sign of the DLM gradient, though we note this is where data are more sparse, and temporal sampling can easily be biased by the large diurnal variability; even so this altitude region appears to be where MLR and DLM are most consistent).

Figure 9 is entirely consistent with, and explains why, Harris et al. (2015) was able to show that the choice of pivot date from the piecewise linear trend using MLR on GOZCARDS, led to larger positive trends the later the date of pivot was chosen, i.e. from 1998 to 2002, most prominently above 10 hPa in both mid-latitude bands (see Fig. 7 of Harris et al. (2015)). We see from the DLM trends in Fig. 9 that at many locations above 10 hPa the gradient is typically zero in 2002, not 1998, especially at 3, 2 and 1.5 hPa, the exact region where the biggest increase in the trend was found by Harris et al. (2015); southern mid-latitude ozone at 1.5 hPa actually appears to start increasing a little later, perhaps in 2004. These results are consistent between all the composites analysed, including the BASIC composite.

It is interesting to note that the two 1998–2012 mid-latitude BASIC composite profiles in Fig. 8, while determined independently of each other, display remarkably similar shapes in the DLM analysis, suggesting a symmetry in the stratospheric driving of ozone changes over this period and, indeed, a similar hemispheric recovery following the Montreal Protocol. In contrast, the lower stratospheric mean-profile changes from MLR (dashed black lines in Fig. 8) are not similar, with a generally (and sometimes statistically significant) positive trend in the southern hemisphere and (an almost significant) negative trend in the northern mid-latitudes.

---

[3]The uncertainties presented in Fig. 9 include an uncertainty on the absolute level in addition to that of the trend, while those presented in Fig. 8 contain only the uncertainty in the trend.
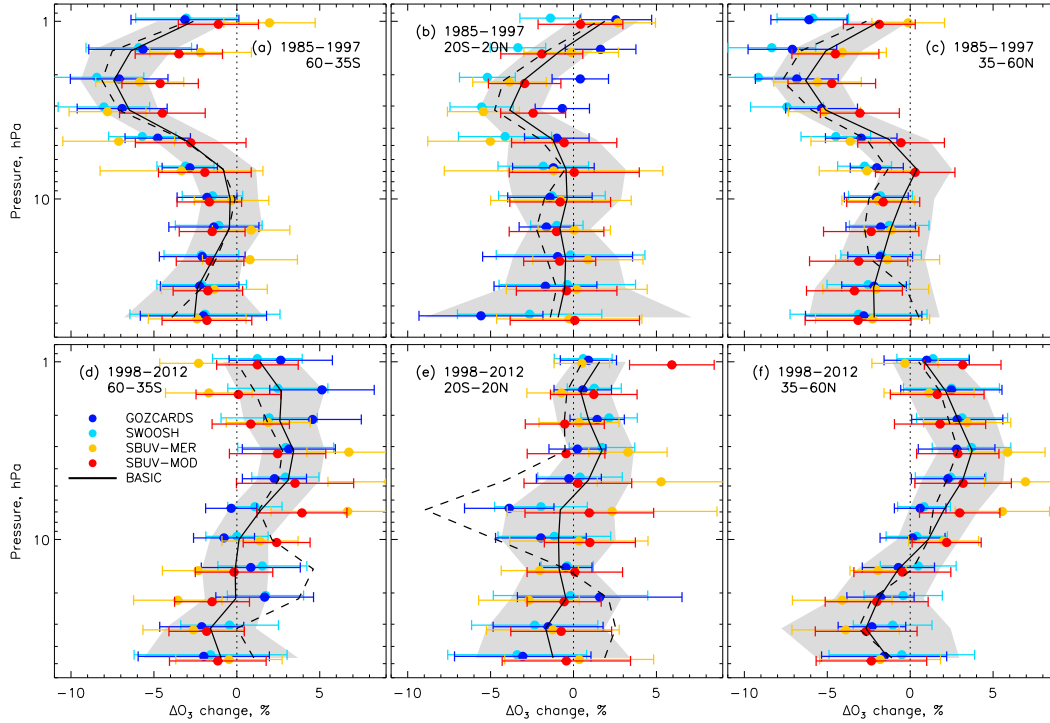
Figure 8: The percentage change in ozone from dynamical linear modelling (DLM) between 1985 and 1997 (upper row) and 1998 and 2012 (lower), over 60°S–35°S (left), 20°S–20°N (middle), and 35°N–60°N (right). GOZCARDS, SWOOSH, SBUV-MER, and SBUV-MOD are shown with error bars representing 95% credible intervals; for the BASIC composite (black), shading represents uncertainties. The mean linear trend estimate from multiple linear regression (MLR) for the BASIC composite is given as a black dashed line (no uncertainties), and is the scaled version of the MLR-BASIC decadal trend shown in Fig. A11.

We propose that the profiles determined by DLM-BASIC are likely to be a better representation of the change in stratospheric ozone than previous estimates. We base this conclusion upon: (i) that the BASIC approach was successful in identifying and correcting most known artefacts in the ozone composites, (ii) the DLM performed better than the MLR in the artificial ozone timeseries test cases, and (iii) the DLM-BASIC outperformed both MLR-BASIC and DLM of all the 'artefact-damaged' artificial timeseries. The consistency of independent northern and southern mid-latitude DLM profiles for both periods would suggest that additional explanation for why the different hemispheres should evolve in different ways is not required (WMO, 2014). However, this also means that further investigation into why MLR and DLM trend estimates can differ so substantially is needed.
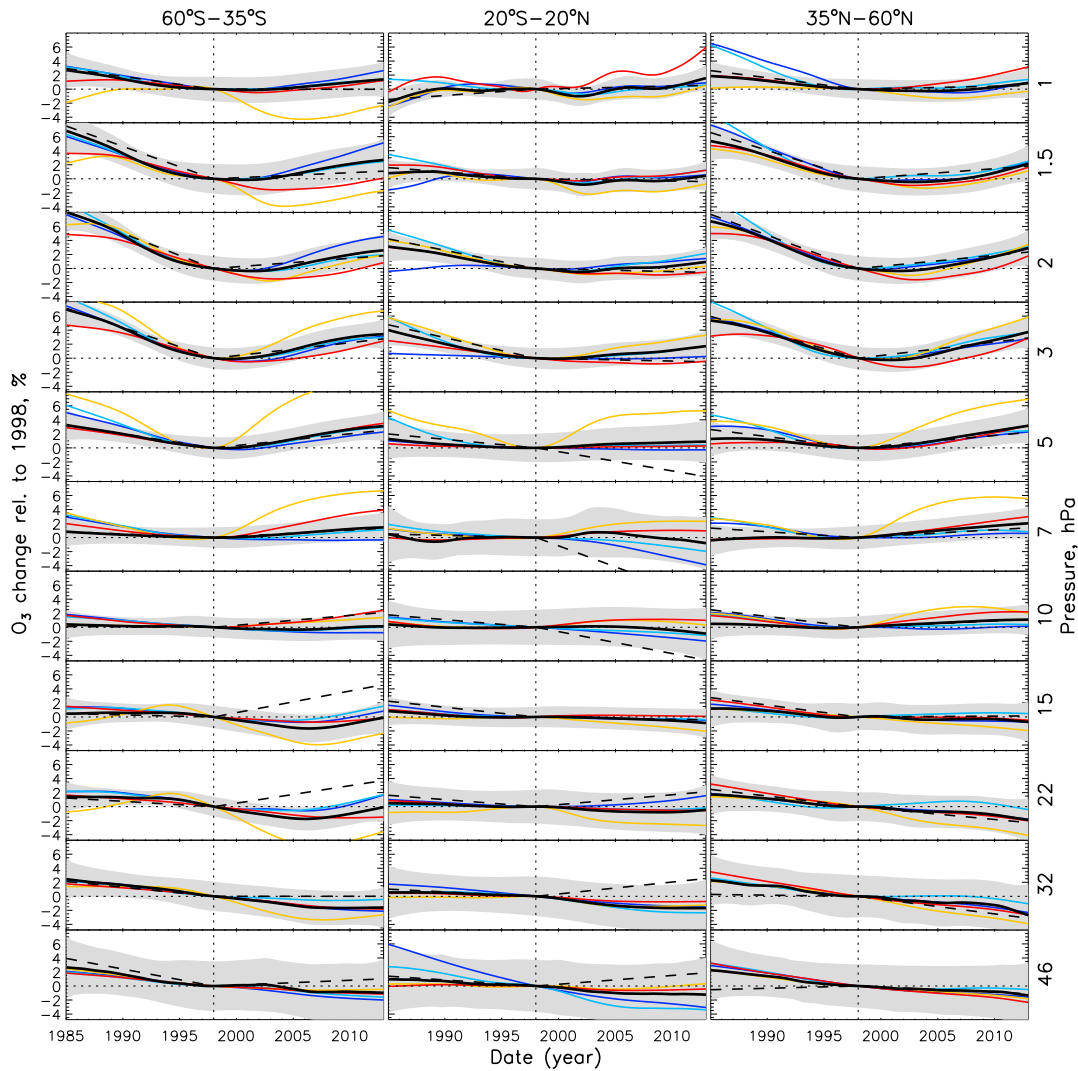
Figure 9: The percentage change in ozone (left axis) relative to 1998 (vertical dashed line; horizontal zero-line) for the integrated latitude-bands 60°S–35°S (left), 20°S–20°N (middle), and 35°N–60°N (right) and pressure levels from 1 hPa (top; right axis) to 46 hPa (bottom). Only the mean trend lines are shown for GOZCARDS, SWOOSH, SBUV-MER, and SBUV-MOD; the BASIC composite is shown in black with shading representing the 95% credible interval. The MLR trend estimates for the period pre- and post- January 1998 are given as dashed-black lines.

6 Conclusions

We have presented a novel approach **to identify and account for data-artefacts that remain in multiple ozone composites of satellite observation. These artefacts are one of largest remain-**
785 **ing causes of disagreement between decadal trend estimates made from the many composites**

available. Our approach includes estimates of uncertainties using singular value decomposition, a Gaussian-mixture outlier-model for the likelihood, and prior information in the form of expected monthly transitions and knowledge of problems in ozone observation; these are combined via Bayesian inference. The main output of this process we term the BAyeSian Integrated

790 **and Consolidated (BASIC) composite, which has been designed to account for differences in ozone composites that are constructed in different ways and with observations from different sources.** The need for better approaches to combine ozone composites has been raised in recent years as an issue needing resolution (e.g. Tummon et al. (2015); Harris et al. (2015)). Harris et al. (2015) stated that it is not currently possible to make definite assumptions about the best way to combine

795 data and in what way, especially when considering multiple composites that use similar, or identical, underlying datasets. Hassler et al. (2014) noted that the key to good estimates of long-term trends is the combination of high-quality measurements and multiple instruments. Our method both requires and benefits from the availability of both. Hassler et al. (2014) further state that the consideration of uncertainties and artefacts is essential, especially when the trends are small compared to the large

800 natural variability (e.g. seasonal cycle), so detailed information is needed about measurement uncertainties, data jumps due to instrument changes, and drifts. Again, our method is specifically designed to address these concerns.

The presence of data gaps, biases between instruments and issues with sampling, noise, and differences in resolution also enhance uncertainties in trend estimates, which might lead to artificial

805 trends being extracted in multiple linear regression (MLR) analysis. To avoid this we employed, with refinements, dynamical linear modelling (DLM) (Laine et al., 2014) and found it to be more accurate than MLR when considering test cases where all variance is understood. The combination of the BASIC approach with DLM shows that the problems listed above can indeed be resolved to improve estimates of ozone changes on decadal timescales.

810 The results presented here are a step forward, but we do not consider the composite a definitive and final product; there are still issues to resolve, which we extensively discuss in the appendix (section A5.2). These caveats include the concern of using the same instrument dataset more than once, even though it may be used in separate composites with different pre-processing (Harris et al., 2015). Our recommendation to resolve this problem, and as the natural next step forward, is to

815 apply the **posterior sampling approach** as a method to combine as many independent datasets as possible, integrating all the known caveats and uncertainties. This will require an additional step to the methodology outlined here in order to account for absolute bias between the datasets, but we do not consider that this will cause significant difficulties.

From the DLM analysis, the estimated changes in ozone between 1985 and 1997, and then be-

820 tween 1998 and 2012, show good agreement with the shape of the ozone profiles presented by Harris et al. (2015), where seven composite datasets were combined with various approaches to estimate errors. The BASIC composite results using DLM (and MLR) show remarkably similar profile shapes

and magnitudes for the earlier period. The implication for the latter period, then, is that ozone is indeed clearly and significantly recovering in the upper stratosphere as a result of the Montreal Protocol, which has not previously been demonstrated universally with significance from observations, though Shepherd et al. (2014) demonstrated that the recovery was indeed underway by removing dynamics that interfere with calculating trends using a model with specified dynamics. The largest uncertainty in the estimates of Harris et al. (2015) came from considering instrument drift. Since the BASIC composite has accounted for much of this uncertainty, we can be confident that our smaller uncertainties represent an improvement. Further, the BASIC composite typically rejects outliers inconsistent with other composites, or otherwise inflates uncertainty estimates, leading to our assertion that the estimated uncertainties are probably a reasonable reflection of the uncertainty in the observations. Uncertainties on the decadal trends can be further reduced with additional regressors, in addition to a new composite based upon independent instrument datasets rather than the four composites we considered here.

We will make the BASIC composite, DLM and MLR trend results available, and will provide supporting documentation should the composite be updated. **The composite will be made available for public use at [to be determined in final version]. In future work we will extend the latitude and altitude range and time period covered, which should lead to more robust results and an improved assessment of ozone trends in the stratosphere.**

Appendix A

A1   Additional information on SBUV-composites

In the construction of SBUV-MER, ozone was considered in 5° daily zonal means and were used in regressions over periods of instrument overlap to account for different variability and combine datasets into the composite; this was also used to identify and account for biases. Specific caveats of the SBUV-MER composite include (see also Fig. 1): (i) the NOAA–11-16 overlap is very short so only a bias offset was applied; (ii) to avoid a propagation of non-physical NOAA-9 trends to the earlier Nimbus-7/NOAA-11 periods, Nimbus-7 and NOAA-11 are not adjusted – this is the major difference between the dataset in Tummon et al. (2015) and the revised dataset used here – only NOAA-9 is adjusted between the two parts of NOAA-11, and NOAA-14 is used as a bridge to the descending part of NOAA-11, but does not appear in the final dataset; (iii) there are large differences in the slope and intercept between 20 and 3 hPa, especially with respect to the adjustment of NOAA–14 to NOAA–11 during the 1997–2000 overlap; (iv) while NOAA–16 and -17 are consistent with respect to SAGE–II instrument observations, the correction approach is not as effective for NOAA–16 and -17 at higher pressures (lower altitudes) at latitudes away from the equator.

In the construction of SBUV-MOD, Frith et al. (2014) looked at offsets in the total column ozone and showed that instruments typically agreed within the stated uncertainty estimates from Monte
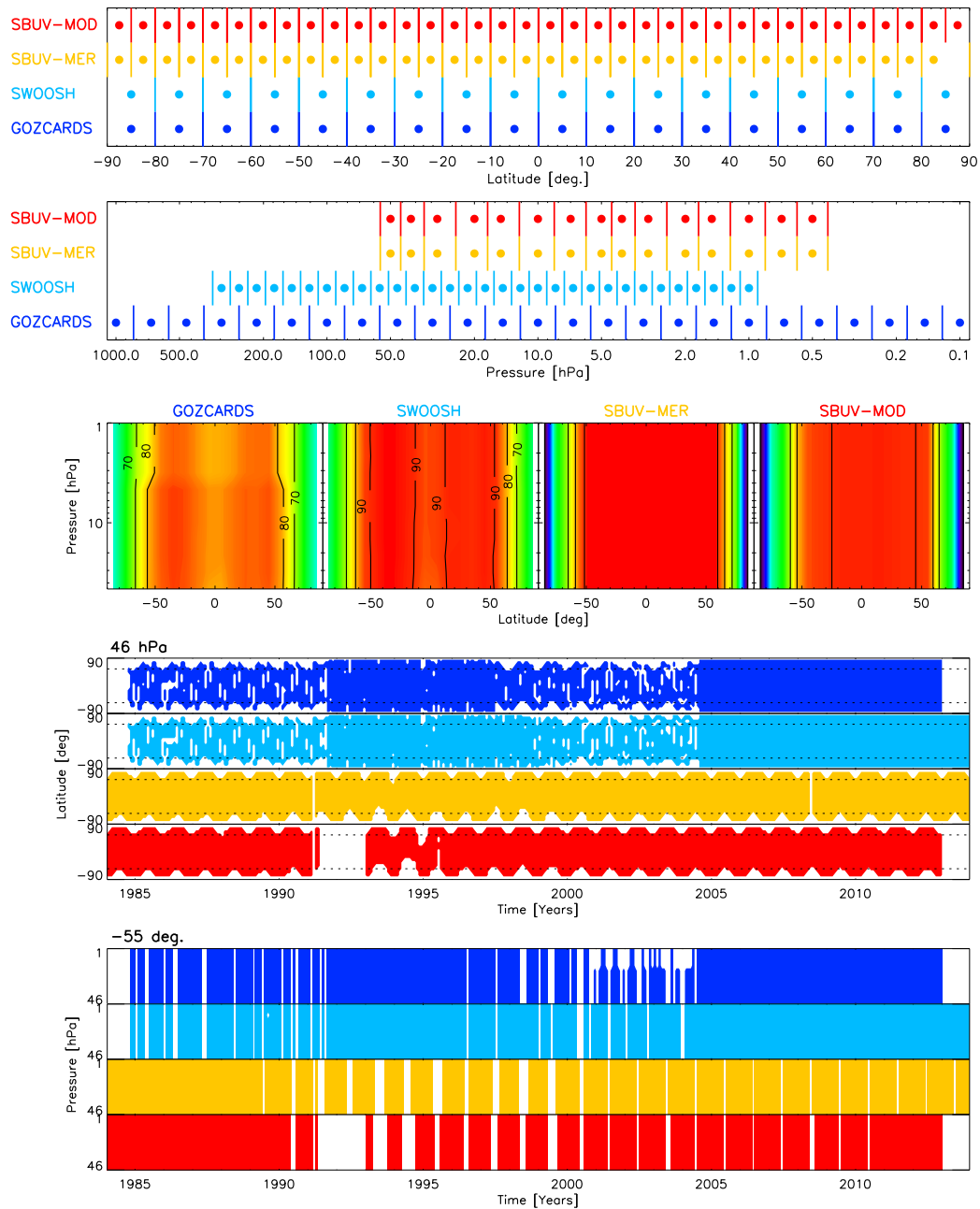
Figure A1: Visual summary of the ozone composites used here. From top to bottom: the latitudinal grid (dots represent the grid centre, lines the boundaries); the vertical grid; the percentage of months between 1985 and 2012 where data are available as a function of latitude and pressure level; the data availability as a function of latitude and time at 46 hPa; the data availability as a function of pressure level and time at 55°S. Apart from the third panel, colours are related to each of the composites: GOZCARDS (blue), SWOOSH (light blue), SBUV-MER (yellow) and SBUV-MOD (red).

Carlo simulations, so no additional offsets were applied to further correct them. Kramarova et al. (2013b) and Labow et al. (2013) had also previously shown that the SBUV total ozone agrees to

860 within 1% with the ground-based Brewer Dobson instrument network, lidar and ozonesondes, and
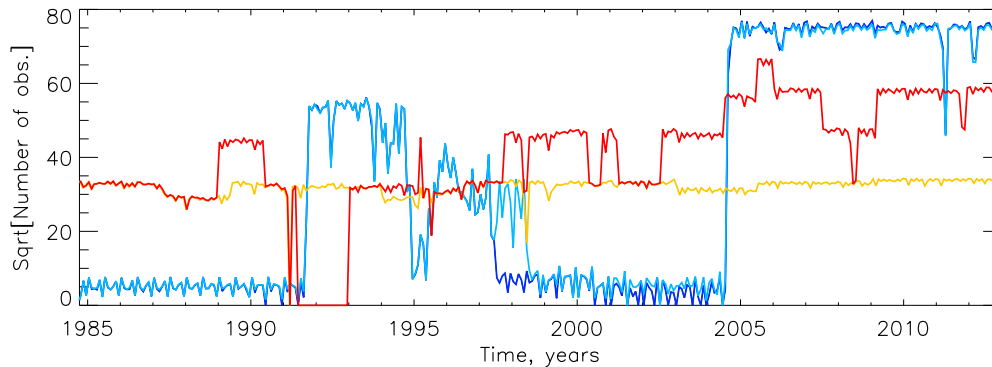
Figure A2: The square root of the latitude-weighted number of observations at 1 hPa between 20°S and 20°N in each of the composites: GOZCARDS (blue), SWOOSH (light-blue), SBUV-MER (yellow) and SBUV-MOD (red).

was consistent with SAGE-II and Aura/MLS satellite observations to within 5%. McPeters et al. (2013) also state that instrument overlaps agree to within ~1% in the globally-integrated (60°N–60°S) total ozone column (TCO), although vertical profiles from NOAA-9, -11 and -14 had the biggest non-random differences of around 2.3% between instruments at 2 hPa, related to orbit drift,

865   data gaps and residual uncertainties, while NOAA–16 and -18 showed differences with standard deviations of ~1.3%. However, despite all of this, it is clear from Fig. 7 of Frith et al. (2014) that they were able to identify offsets in the TCO - these offsets mimic the structure of the offsets between the SBUV-composites we show in Fig. 2c, indicating that while small in total column, they are on the order of 5% in the vertical profile, vary in magnitude and sign throughout the atmosphere, and

870   potentially mask offsets in the integrated column.

     Kramarova et al. (2013b) and DeLand et al. (2012) also have shown that the 1994-2000 period is of worse quality than earlier and later periods (Frith et al., 2014); DeLand et al. (2012) recommend that NOAA–9 should not be used, which is why NOAA–14 is used for this period in SBUV-MOD, although NOAA-11 drifts from 4pm to 6pm during the 1994–1995 period, for which NOAA–9 is

875   alternatively used in SBUV-MER. A quality 'tier' for the satellites was provided in (Frith et al., 2014), which is useful in the compilation of the SBUV TCO Merged Ozone Dataset, with drifts tending to cancel in NOAA–11 and –14 overlaps from 1997–2000 in TCO, but this does not reveal the profile uncertainties and drifts. The use of the priors for the BASIC composite was necessary to identify and account for the drifts.

880   **A2   Additional information on the SAGE-composites**

Due to the low temporal sampling of SAGE-II (15 sunrise/sunset events per day), as opposed to the 3500 limb emission profiles per day from Aura/MLS, binning of data in GOZCARDS is done into 10° latitude averages, and datasets are connected by accounting for biases between dataset overlaps. It should be noted that biases always exist between instruments due to calibration, spatial

885   and temporal sampling, profile resolution, signal variability or retrieval errors. For example, Toohey

et al. (2013) showed that occultation sampling errors with respect to emission measurements could reach 10–15% at high latitudes when atmospheric variability was large. The processing procedure, which occurs before data are binned into latitudes, attempts to remove outliers and impacts from clouds or aerosols and they do not disregard data arbitrarily or attempt to fill in spatial or temporal gaps. The impact of using SAGE II v6.2 instead of v7.0 is discussed by the GOZCARDS team (Froidevaux et al., 2015), which shows very little systematic differences in number density, but leads to large differences when converted to vmr with temperature from either NCEP or MERRA (as confirmed by (Maycock et al., 2016; McLinden et al., 2009)). We note that small drifts of ~0.5% yr^{-1} do exist between HALOE, SAGE II and Aura/MLS (Nair et al., 2012; Kirgis et al., 2013), and Nazaryan and McCormick (2005) and Hubert et al. (2016) suggest that most the datasets used in GOZCARDS have good stability.

In SWOOSH, basic data pre-screening is based on published recommendations from satellite instrument teams. SAGE–II ozone screening follows the recommendations of Wang et al. (2002) to remove aerosol contamination and poor quality retrievals; any profile containing more than 10% uncertainties between 30 and 50 km are removed. SWOOSH also applies additional screening for profiles before November 1992 affected by the Mt. Pinatubo eruption, using information from the NO observing channel. Offsets applied to the non-reference instrument data vary only by pressure and latitude but not time, such that if drifts exist they may not be accounted for in SWOOSH, and GOZCARDS.

We briefly note (and indicate in Fig. 1) technical details in the construction of the SAGE-based composites: (i) for GOZCARDS there are no months where SAGE-II and ACE-FTS overlap in the NH-tropics due to ACE-FTS coverage being poor; (ii) McLinden et al. (2009) noted that UARS/HALOE and MERRA confirm that there were artefacts in SAGE-II after 30 June 2000, so these data are not used at altitudes above 3.2 hPa; and (iii) problems with the SAGE-II azimuth gimbal in mid-2000, and corrected by November, meant there was only a 50% duty cycle during that period, when it already took about a month to collect data to fully cover latitudes 80°S to 80°N.

A3 Additional information, results, and discussion on the BASIC approach

A3.1 Effect of the Box-Tiao equation

In the Fig. A3 we show 25 plots, for five values of γ combined with five values of β. In this plot we imagine an idealized scenario of four composites in one month with mean values at -1.5, -1, +1, and +1.5, all with an uncertainty of σ=0.2.

It is clear that for either low values of γ, and/or low values of β, we get the expected result assuming all data are independent (which is the dotted line in all plots), but this is inadequate as such a pdf (dotted line/black thick line) does not represent any of the data and is in a region of low probability. For large values of β and γ (top right) we end up with belief in any of the

data points being low (i.e. we enhance σ^2 by a factor of γ^2) with any affect from the second (separation) term beginning with (1-β) killed off by $\beta \sim 1$; clearly this scenario is not what we are looking for. As the aim is to essentially enhance regions where data agree and reduce belief in outliers, the preferred region of interest is for intermediate values of β (0.1–0.9) and $\gamma > 10$. From this, we choose $\beta = 0.1$ and $\gamma = 100$ as this appears to reflect well the desired separation into a multi-modal pdf that represents two independent sets of data (e.g. blue and red/yellow groups).

In terms of its effect on the BASIC composite timeseries, when combined with a prior expectation, this can lead to the expected timeseries following one pair (in the example given in Fig. A3) after it has become clear that a jump/offset has occurred, whereas low γ or low β leads to getting an average of all the composites with a bias introduced by the prior.

A4   Additional information on DLM parameter estimation

In Figs. A4–A7 we show the recovered posterior distributions for the DLM nuisance parameters {σ_{trend}, σ_{seas}, σ_{AR}, ρ_{AR}} resulting from the DLM analysis of the BASIC composites performed in section 5. In the case of σ_{trend} (Fig. A4), the posteriors (red) are shown against the applied half-Gaussian priors (blue). In this case, the choice of prior is particularly subjective – in the case where σ_{trend} is allowed to attain large values the DLM can collapse into a case where the "trend" has so much freedom it can follow the data exactly and capture all variability. Therefore, it's necessary to choose a sensible upper-limit on σ_{trend}, ie., on the maximum allowed variability of the smooth background trend. In this study we chose for the prior on σ_{trend} a half-Gaussian, centered on zero, with dispersion 0.0005. All other parameters are given uniform priors.

A5   Success of BASIC approach in accounting for artefacts between composite versions

BASIC composite results in the main article uses SWOOSH data version 2.6. We originally used version 2.5 (version 2.1 was used by Tummon et al. (2015) and Harris et al. (2015)), which was updated to account for an error which led to Aura/MLS being offset in absolute terms by one vertical level. This artefact was clear in our original analysis, and we present an example here to show that the BASIC composite constructed with four composites is relatively unaffected by these types of artefacts.

In Fig. A8, we show the same results for the BASIC composite (black) and SWOOSH version 2.6 (light-blue) as in Fig. 6a and b at 2.2 hPa and 0–10°N. In addition, we also show SWOOSH v2.5 (purple) and in red the BASIC composite based on the same input data, but with SWOOSH v2.5 instead of v2.6 ('BASIC(SWv2.5)'). Prior to 2004 the SWOOSH v2.5 line is offset by ~+0.3 ppm from the zero line (i.e. relative to BASIC) and SWOOSH v2.6 in Fig. A8b. While there are small variations in the BASIC(SWv2.5) (red line), it also sits close to the zero line, typically with an
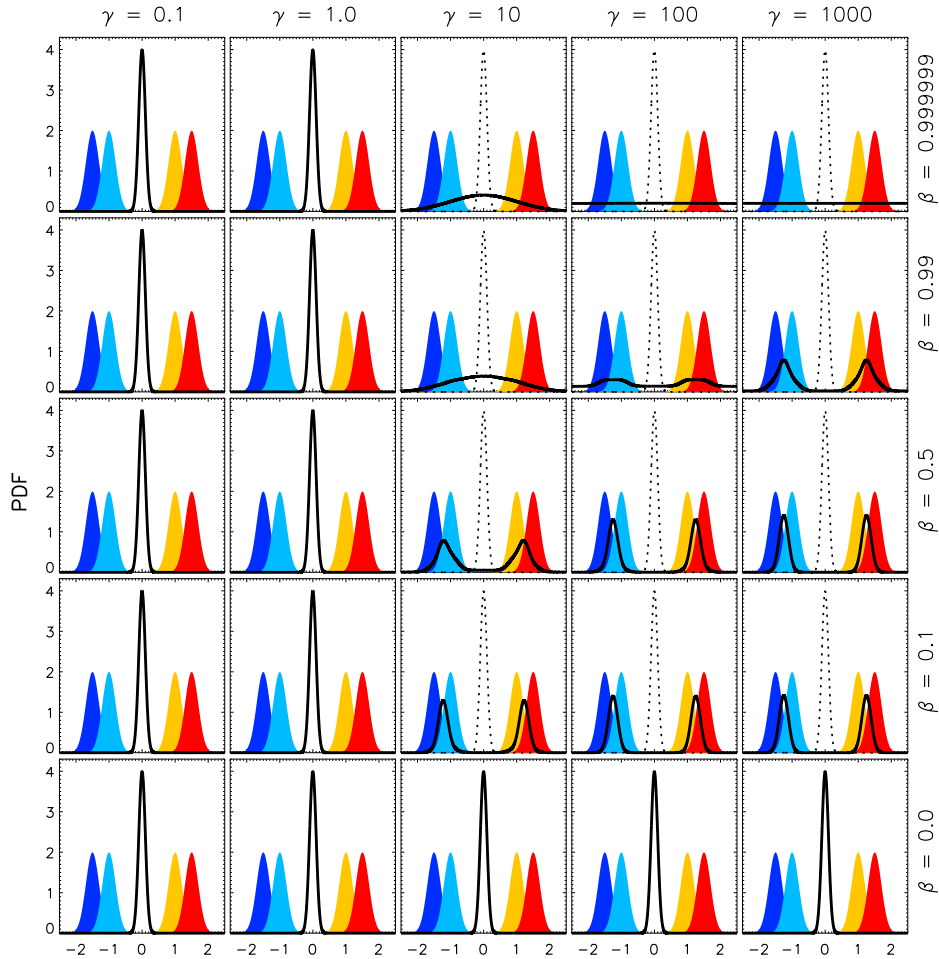
Figure A3: Example of Box-Tiao effect on idealised data with a mean of -1.5, -1.0, 1.0 and 1.5, blue, cyan, yellow and red, respectively, all with the same uncertainty σ=0.2. Dotted lines in all plots represent the pdf resulting from multiplying all data treating them as independent. The solid black line represents the pdf following the Box-Tiao equation. Values of γ and β used in the Box-Tiao equation in each plot are shown along the upper and right axes.

offset of ~+0.05 ppm and ranges between zero and ~+0.1 ppm. We find that the BASIC composite is similarly unaffected by offsets in the previous version of SWOOSH at other locations.

This example gives us further confidence that when multiple composites are available the BASIC approach does a good job of accounting for artefacts that exist in only one dataset.

960 **A5.1 Test of BASIC approach using artificial timeseries**

Given that we do not have any **certain** measurements against which to test our approach we need to demonstrate how the BASIC approach operates in ideal, known conditions, by using artificial tests
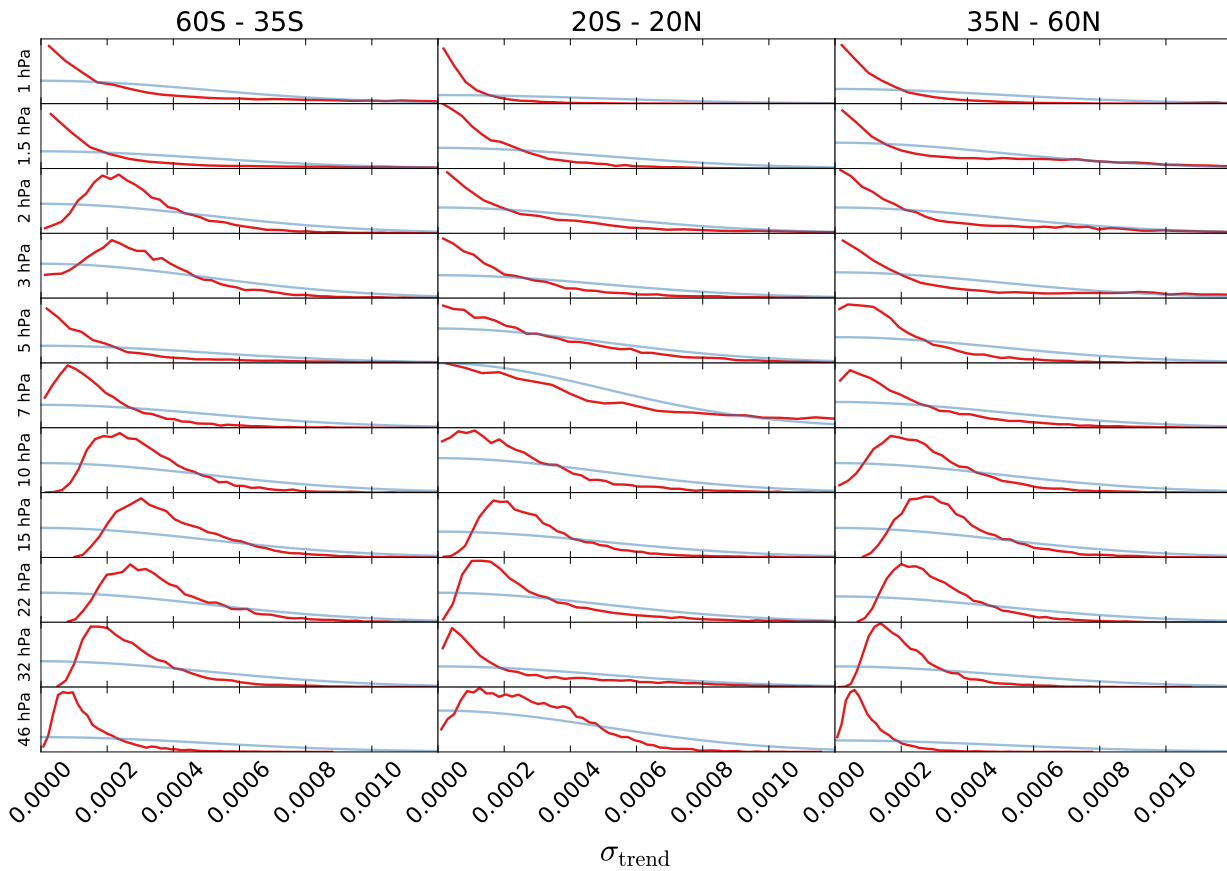
Figure A4: Recovered posteriors on σ_{trend} (red) and the chosen half-Gaussian prior with dispersion 0.0005 (blue) from the DLM analysis performed in section 5.

cases where all the variance is understood. With that in mind, we designed three sets of tests; we present one here and consider DLM and MLR analysis on the other two in section A6.

965   To create test cases, we took a real ozone timeseries, and from that estimated the regression coefficients of, solar, ENSO, volcanic aerosols, and two QBO terms using MLR (as in section 5.1), and then reconstruct the ozone timeseries with these known regressor coefficients, in addition to a realistic seasonal cycle based upon similar variability in the observations. We add a Gaussian noise term, but drop unknown residual variance. To represent instrument artefacts and drifts similar to the

970   situation we have here with the SAGE- and SBUV- composite pairs, we produce artefact timeseries that are different between pairs, with some other differences within the pairs - these are shown in Fig. A9b as the straight lines. We add these, with different realisations of Gaussian noise for each 'instrument', to the artificial time series to produce the 'damaged' ozone timeseries shown in light-blue, blue, red and yellow in Fig. A9a. We then proceed by applying the BASIC approach to the

975   four 'damaged' timeseries exactly as with the real ozone timeseries/composites; the result is shown in black with the 95% credible interval in Fig. A9a. The difference of the four artificial timeseries, relative to the undamaged ozone timeseries (not shown), are shown in Fig. A9b.
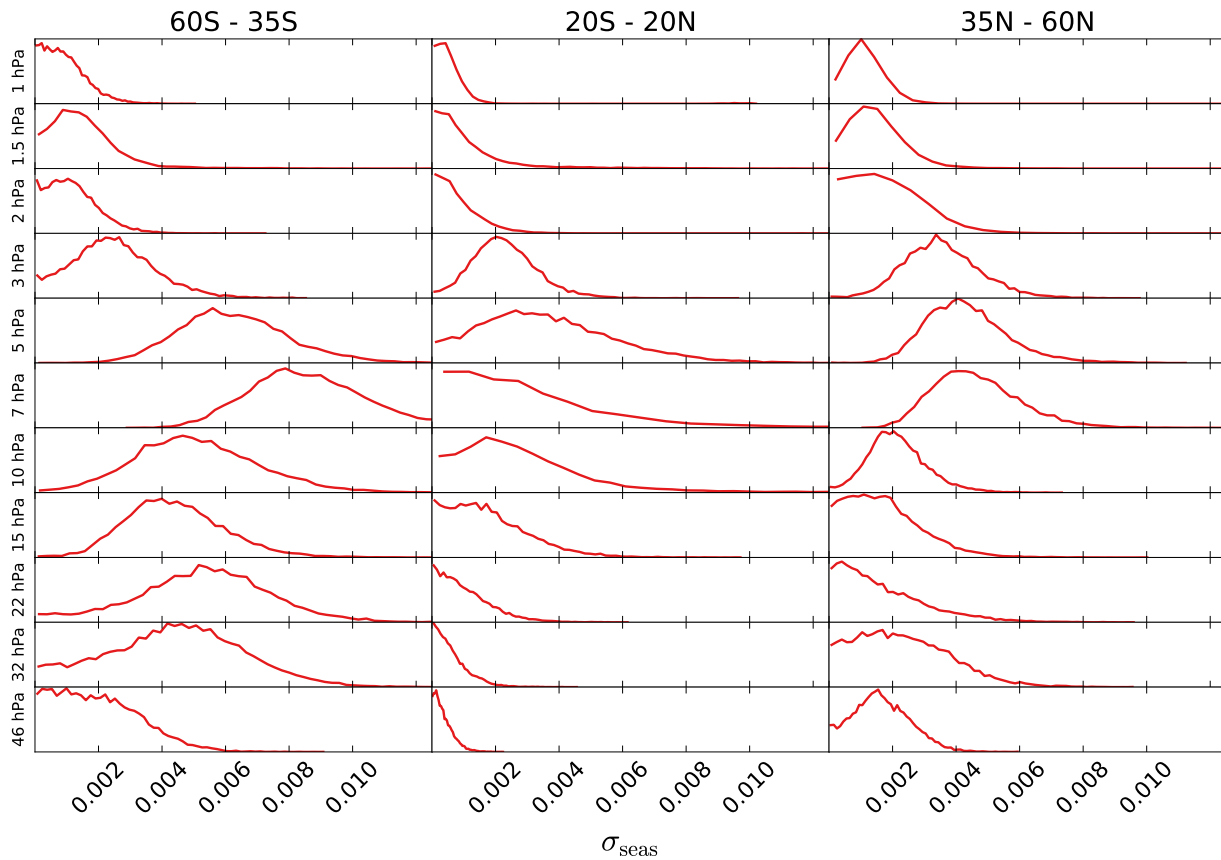
Figure A5: Recovered posteriors on σ_{seas} from the DLM analysis performed in section 5.

We specifically built the artefact timeseries to provide difficulties for the BASIC approach. For example, in Fig. A9b at around month 50 all the damaged timeseries disagree with the undamaged, target ozone timeseries in the same direction, to show that the BASIC algorithm is unable to reproduce the undamaged ozone timeseries if none of the observations/composites correctly represent ozone during this period. Thus, if all observations are wrong, there is nothing that can be done to resolve the issue, other than modeling using e.g. a chemistry climate model. After month 250, all the datasets are the same (i.e. there are no artefacts except the Gaussian noise that simulates instrument noise and pre-processing differences) and the BASIC approach naturally matches the artificial timeseries during this period. Prior to month 170, only one pair is either drifting or has a jump, but not both at the same time, though they are all typically offset from the target: during this period, except when all four are different from the target (~month 50), the BASIC result generally matches the expected ozone within the 95% credible interval. The period between month 170 and 210 was designed to be complex, with drifts and jumps occurring within and between pairs in rapid succession. The BASIC result, unsurprisingly, does not perform so well during this period though it doesn't generally deviate too far from the target; between 200 and 250 it is closer to one pair, but sits between all four since there is roughly equal information and uncertainty in each of them. Throughout, when the
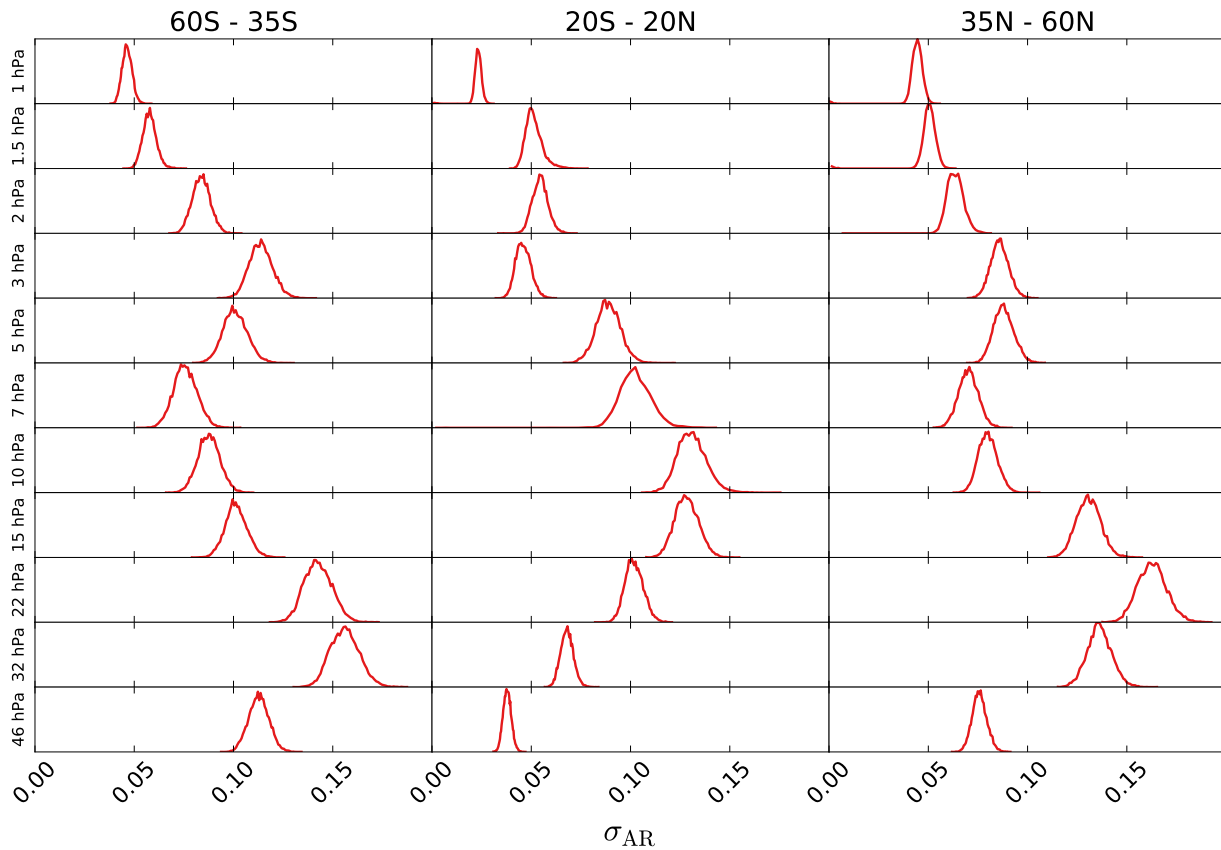
Figure A6: Recovered posteriors on σ_{AR} from the DLM analysis performed in section 5.

artificial timeseries are far apart, the BASIC result uncertainties typically increase to accommodate
995 the higher uncertainty.

A5.2 Caveats on using the BASIC approach

So far, we have discussed several drawbacks with the current version of the BASIC approach presented here. Here we collate and list these, and briefly discuss potential solutions for the future, where available.

1000 1. **Vertical resolution:** This is a problem related to the different averaging kernels of the various instruments used to construct the composites - the SAGE-composites use instruments that all have higher resolution than those in the SBUV-composites. This difference in vertical resolution becomes more important at lower altitudes, and it is clear in the case of the QBO signal being different (Bhartia et al., 2013). Kramarova et al. (2013a) recommends only using the
1005 integrated column from SBUV data below 25 hPa (16 hPa between ±20°), because although SBUV is sensitive to ozone in the troposphere and lower stratosphere, the vertical distribution of that ozone is determined by a priori constraints. Alternatively, when making direct comparisons between SBUV and other high vertical resolution instruments (e.g. Aura/MLS), Bhartia
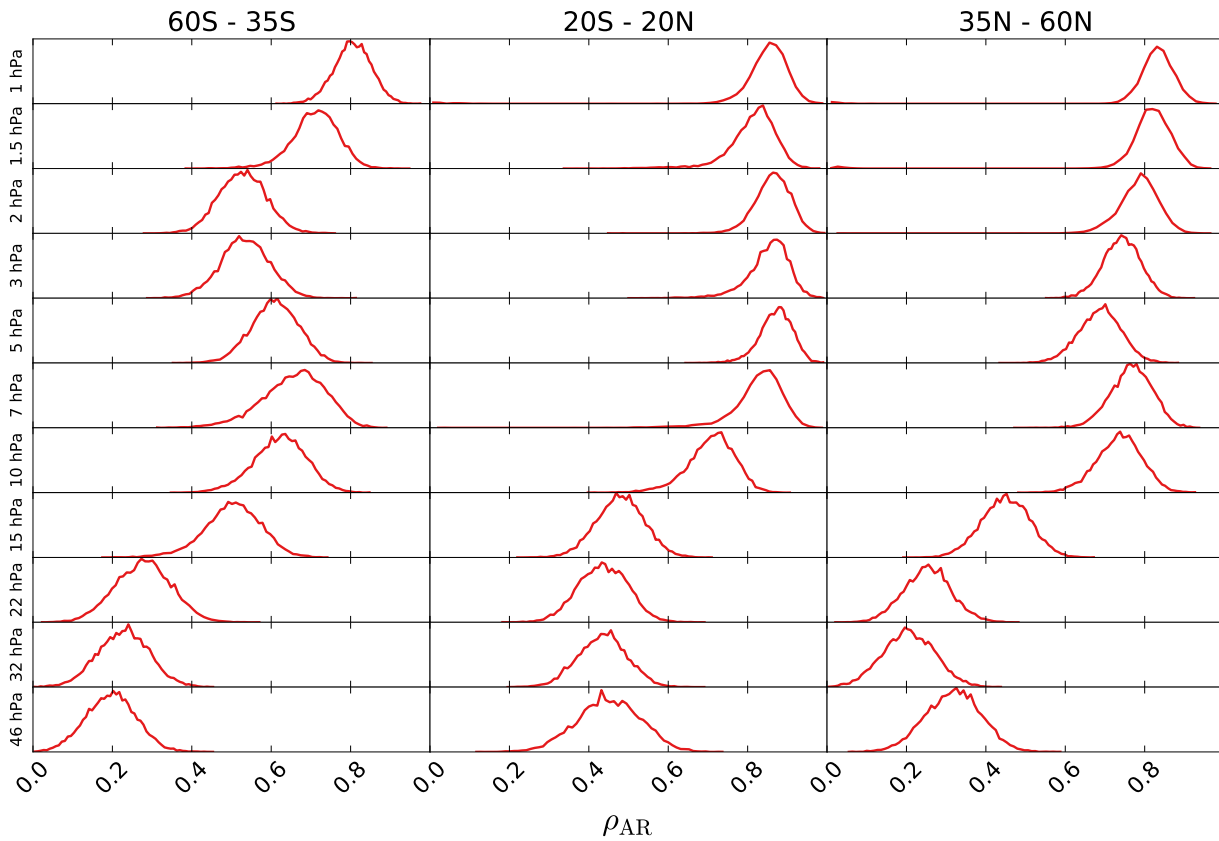
Figure A7: Recovered posteriors on ρ_{AR} from the DLM analysis performed in section 5.
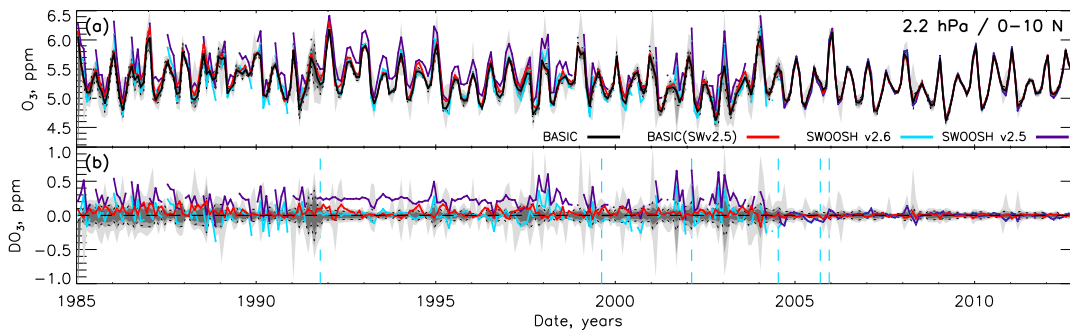
Figure A8: Ozone timeseries from 1985–2012, all bias-shifted to the mean of SWOOSH v2.6 after August 2005. (**a**) Absolute ozone at 2.2 hPa over 0–10°N from SWOOSH v2.6 (light-blue), SWOOSH v2.5 (purple), BASIC using SWOOSH v2.5 (red), and the BASIC composite using SWOOSH v2.6 (black, with shading representing 68% (dark-grey), 95% (grey) and 99% (light grey) credible intervals (CIs), and 2 standard deviations (dotted lines)). (**b**) As for (a), but for the difference relative to BASIC(SWOOSHv2.6).
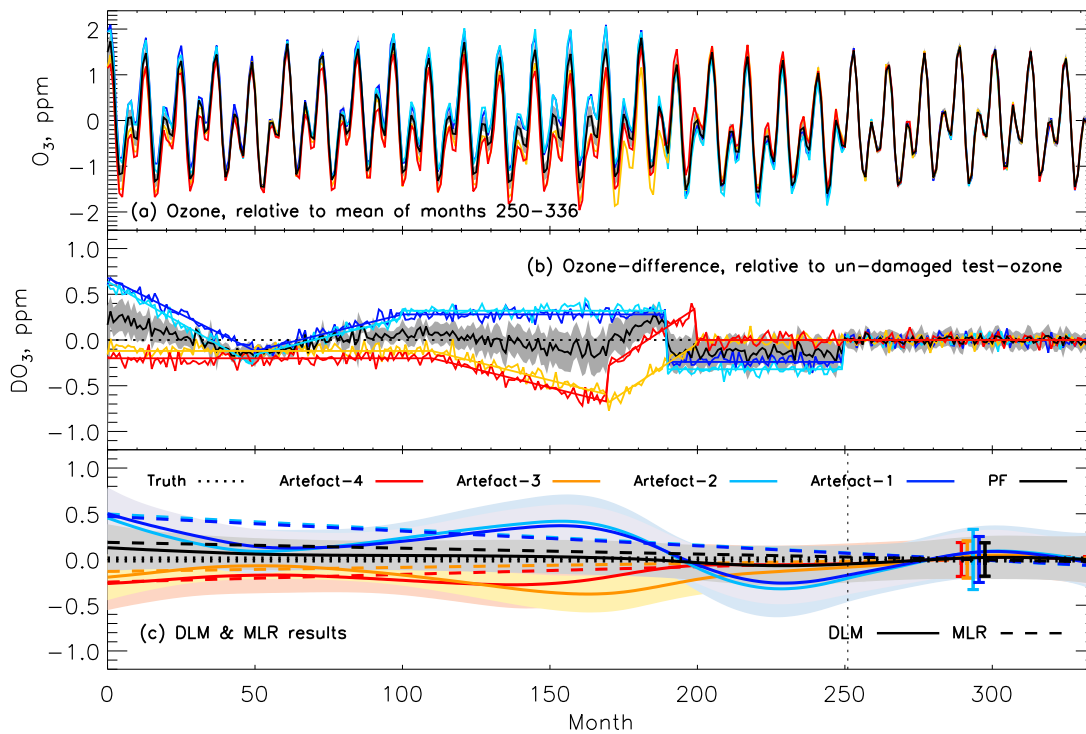
Figure A9: A test case to evaluate the performance of the BASIC approach. Damaged timeseries are plotted in (a) relative to the mean of months after 250 in light-blue, blue, yellow and red, and the BASIC result in black. Differences of timeseries in (a) relative to the undamaged (test) timeseries is shown in (b); the straight coloured lines in (b) represent the artefacts applied to the undamaged timeseries to produce the damaged ones in (a); grey and shading in (a) and (b) represent the 95% credible intervals of the BASIC result. In (c), we show the estimated trends over the full period from multiple linear regression (MLR; dashed) and the dynamical linear model in solid lines. The true trend during this period is zero (dotted line).

et al. (2013) advise using the SBUV kernels to degrade the resolution of the instrument to
match the vertical resolution of SBUV before comparing. However, given that some issues with resolution are already evident at 10 hPa (Fig. 6), and that there is still some useful information in the ozone observations below 25 hPa, we still consider the data relevant in this study. This issue should not represent a significant problem when MLR or DLM analyses are performed since the two QBO regressor terms should capture much of the QBO variability. However, if one is interested in the QBO itself, then we would also recommend using the SAGE-based composites and/or datasets used to construct them (see also Kramarova et al. (2013a)). We would not endorse a solution based on de-weighting a composite relative to its vertical resolution, because then SBUV will always be at a lower weight than the SAGE-composites and the BASIC approach will always favour the latter.
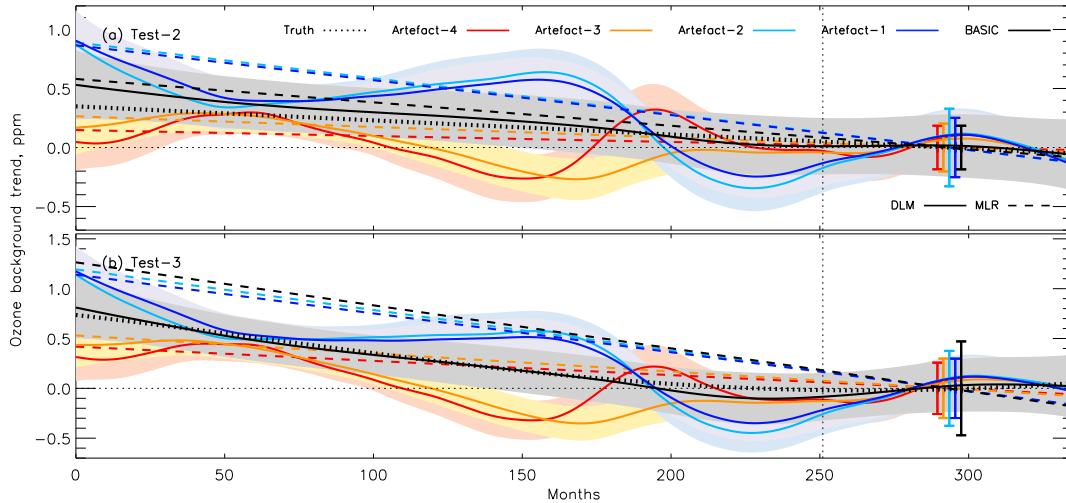
Figure A10: Similar to Fig. A9c: two additional tests cases where the only change is that the background trend in (a) is linear and in (b) non-linear, as shown with the thick-dotted black line.

2. **Double-counting:** The use of only two pairs of composites, each built using the same underlying instrument data, resolves one of the concerns of Harris et al. (2015) about biasing our result towards the composites with the most common instrument data (e.g. five of the seven composites combined by Harris et al. (2015) used SAGE-II as a major component). However, this leads to the problem that for periods when two of the composites are identical (i.e. not offset and with similar artefacts), the likelihood estimate may be biased in favour of that pair, which are being treated as independent datasets when indeed they are not. An example can be seen in Fig. 6b prior to 1991, where the SAGE-composites are offset from each other, but the SBUV-composites are at almost identical levels. It is fortuitous that the level of SBUV is in close agreement with SWOOSH before and after 1991, but this may not be the case in other locations. In reality we should not treat the SBUV data as independent during this early period, but this adds further complications in making decisions about when they should be considered as independent or not. We choose not to make this decision as this removes much of the objectivity that the BASIC approach provides. To account for this in future we recommend that the approaches put forward here should be applied to the original datasets underlying the composites, each considered independently but with prior information, to construct a composite. This would require an additional step to estimate the offset between datasets, and to assign one dataset as a reference, but this would be a relatively straightforward addition to the procedure.

3. **Restricted altitude range:** We currently only consider the pressure range 47–1 hPa (~20–48 km) as we are restricted to those covered by all the composites. The GOZCARDS and SBUV-composites go higher, but observations in this region are subject to rapid diurnal changes that require good geo-location and temporal sampling, and the local time of the observations must

be taken into account. MLR trend analysis (Fig. A11) shows that the composites can display significant different long-term behaviour at 1.5 and 1 hPa, even between pairs of composites (though this is less the case using DLM in Fig. 8); this is also where diurnal variability is a serious issue as mentioned by all groups in either publications or user documentation (e.g. see McPeters et al. (2013); Davis et al. (2016) and references therein). This is an issue that is still being investigated by the community, and we do not address it here. However, in addition to pre-screened data, it may be something that is possible to resolve with accurate transition-priors, and additional prior information, in addition to the ones we already suggest using here. Observations are also available down to 316 hPa, but there are large gradients in ozone at these levels, so even the relatively high resolution of the instruments in the SAGE-composites can struggle to accurately resolve variability at individual layers this low down. However, many observations do exist, and so when integrating the original data using the BASIC approach (see previous point), these layers could be included, and additional prior information could also be used to account for the large ozone gradients.

4. **Restricted latitude range:** While the composites extend to higher latitudes than 60°, at these latitudes the need for direct or scattered sunlight leads to several months of the year where data are missing, with increasing periods of the year without observations closer to the poles. We do not attempt to fill these data without observations available. In future, we could use night-viewing instruments such as GOMOS (Kyrölä et al., 2013), to extend into higher latitudes when these data are available (i.e. after 2002), but it is not possible to do it prior to the GOMOS measurements, except potentially through ground-based observations, though they are usually limited to lower altitudes than the satellite observations can consider. In future we could also consider extending the BASIC approach to better estimate ozone during at least the summer seasons.

5. **Mt. Pinatubo: The example given at 10 hPa, and checks at other locations, clearly indicates that the BASIC approach is able to avoid the artificial decrease in the SBUV-MER data between June 1991 and 1992. Frith et al. (2014) advise caution when using data in the 6–9 months following the eruption, especially for 15°S – 30°N. Thus for this altitude, when using MLR to analyse trends, we also advise caution during this period because the SAGE-pair dominate during this period and if Pinatubo eruption related artefacts remain in these data they will influence the BASIC composite during this time. One idea to consider would be to increase the prior de-weighting factor over this period, but this would be an additional subjective decision, so we prefer to flag this information instead and find a more elegant solution in the future. However, such a problem may not be possible to resolve if the eruption inherently affects observations which cannot be removed prior to applying the BASIC algorithm.**

Some of these caveats may be resolved with additional information from the ozone community and by using the BASIC approach to construct a composite from the original, individual instrument timeseries. Nevertheless, for the work involving composites here, we conclude that despite these issues, overall the BASIC approach performs well in estimating ozone variability. This conclusion is based upon the artificial test case target timeseries being well estimated, the results of the example real ozone timeseries presented in Fig. 6 that account for known issues, and the success in the case of the SWOOSH version changes where the BASIC approach accounts for the problems in SWOOSH in v2.5 in advance of the v2.6 release (section A5).

A6   Comparison of multiple linear regression and dynamical linear modelling in estimating long-term trends

To test the ability of MLR and DLM to estimate the background trend, we use the artificial test cases presented in appendix section A5.1 and Fig. A9a, in addition to two more with the same regressor-coefficients and noise, but with a linear and non-linear time-varying background trend (Fig. A10). The first set have a background, linear, zero-trend (Fig. A9c), the second a linear downward trend (Fig. A10a), and the third a downward-linear trend plus a non-linear curve that reaches a minimum in the latter half of the full period before increasing again (Fig. A10b); the true 'target' trends are shown in Fig. A9c and Fig. A10a and b as thick-dotted black lines. In each case we apply the BASIC approach to the four sets of artefact-damaged timeseries, as in Fig. A9. Therefore, we have 15 test timeseries, all fully understood. This does not represent the situation for the real ozone timeseries since in many of those cases the MLR residuals (unaccounted for variability) can typically account for ~50% of the variance. However, these tests with artificial ozone timeseries are indicative of the performance with real timeseries.

One major advantage of DLM over MLR for estimating long-term trends is that MLR requires the trend to be prescribed in advance as linear, or piece-wise linear trends (e.g. Kyrölä et al. (2013), or is expected to follow the equivalent stratospheric chlorine (EESC) curve (Newman et al., 2001). The shape of the EESC, which follows CFC stratospheric loading that peaked in the mid-to-late 1990s, impacts more on the sensitivity of the MLR analysis than the period length does when calculating decadal trends WMO (2011). The main problem in assuming an EESC shape is that the timing of chlorine minimum is location dependent with, e.g., higher latitudes lagging those closer to the equator since it takes time for chlorine changes to reach different regions. Therefore, fixing the decline date may lead to misleading estimates (Harris et al., 2015). The use of the DLM allows this issue to be circumvented to some degree by not fixing the background trend or an inversion date (Laine et al., 2014) and allowing it to vary with time, though this still does not necessarily separate EESC from dynamical changes related to, e.g., changes in the BDC (Polvani et al., 2011; Harris et al., 2015).

In Fig. A9c, we plot the MLR (dashed) and DLM (solid) trend results[4]. In this example the true long-term trend is zero (dotted black line). **The only result that is able to stay within two standard deviations of the 'truth' is the DLM of the BASIC result, and usually it is within one standard deviation. The MLR of the BASIC result shows a significant downward trend, and naturally one would not expect the MLR of the damaged timeseries to estimate an accurate result. What is interesting to observe is that the DLM accurately extracts the drifts in the damaged background trends as well, which might be useful in future studies to further assess anomalous behaviour in the composites by interpreting the behaviour of the DLM results from each composite. The two tests with the linear and non-linear background trends (Fig. A10) lead to essentially the same conclusions, with the non-linear trend being fitted almost exactly, while MLR is significantly off from the 'truth'. A more thorough assessment of the DLM with respect to MLR will be made in a forthcoming publication.**

In summary, our tests suggest that when estimating the long-term trend, the use of the BASIC approach to correct data, together with the DLM, is more successful and accurate than using MLR or DLM on uncorrected timeseries. Therefore, we would recommend using the BASIC approach combined together with the DLM for the analysis of long-term trends in ozone, as outlined in this study.

Acknowledgements. **We thank the referees, Daan Hubert and Marko Laine, for their thorough input which lead to significant, but important changes that strengthened the paper as a result.** We also thank S. Frith, J. Wild and L. Froidevaux for detailed comments on the composite datasets and general comments on the manuscript. We also thank the GOZCARDS, SWOOSH, SBUV-MOD and SBUV-Merged Cohesive composite teams for use of their data. W. T. Ball and E. V. Rozanov were funded by Swiss National Science Foundation (SNSF) grants 200020_163206 (SIMA). Fiona Tummon was funded by SNSF grant 20F121_138017. GOZCARDS ozone data can be found at https://gozcards.jpl.nasa.gov/. SWOOSH ozone data can be found at http://www.esrl.noaa.gov/csd/groups/csd8/swoosh/. SBUV ozone data can be found at http://acd-ext.gsfc.nasa.gov/Data_services/merged/. **The BASIC composite will be made available following the review process and this sentence will be replaced with information regarding its location.**

---

[4]**Note that in these test cases for our DLM inference we assume a half-Gaussian prior on σ_{trend} with dispersion 0.001 rather than 0.0005. This is for illustrative purposes, to emphasize the impact of "damaging" the time series on the recovered trend, and we note that the choice of prior on σ_{trend} is in any case subjective (see section A4).**
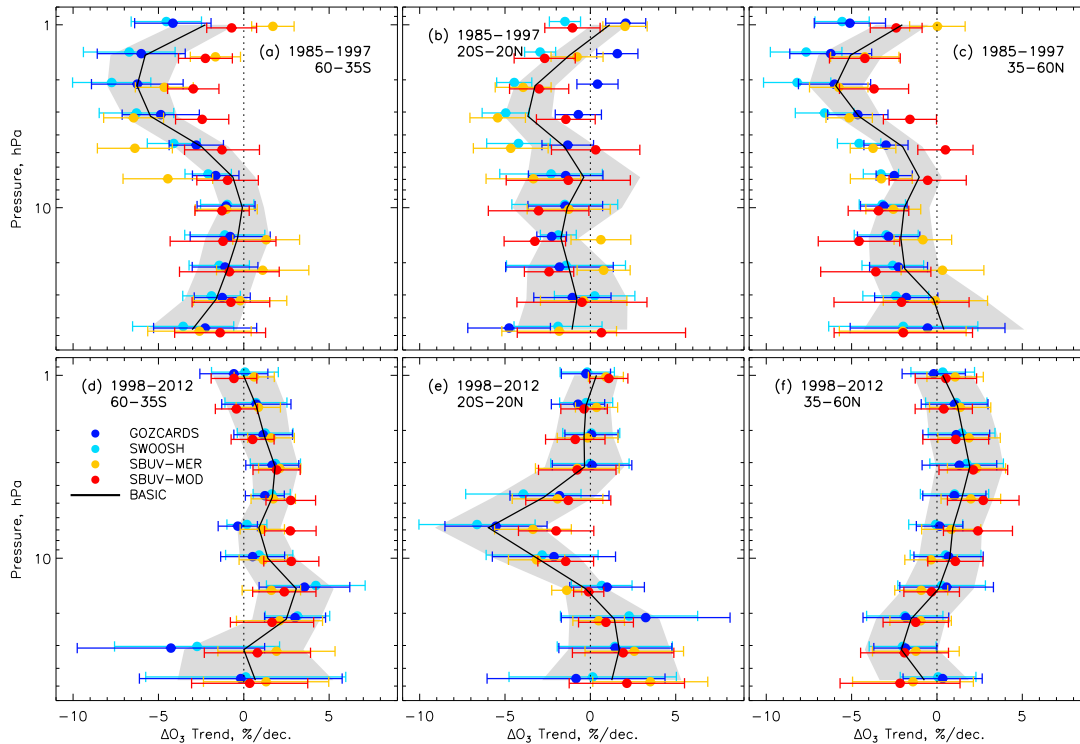
Figure A11: The decadal trend in ozone from multiple linear regression (MLR) between 1985 and 1997 (upper row) and 1998 and 2012 (lower), over 60°S–35°S (left), 20°S–20°N (middle), and 35°N–60°N (right). GOZCARDS, SWOOSH, SBUV-MER, and SBUV-MOD are shown with 95% credible intervals; the BASIC composite is shown in black with shading representing 95% credible intervals.

References

Adams, C., Bourassa, A. E., Sofieva, V., Froidevaux, L., McLinden, C. A., Hubert, D., Lambert, J.-C., Sioris, C. E., and Degenstein, D. A.: Assessment of Odin-OSIRIS ozone measurements from 2001 to the present using MLS, GOMOS, and ozonesondes, Atmospheric Measurement Techniques, 7, 49–64, doi:10.5194/amt-7-49-2014, 2014.

Arnold, S. R., Methven, J., Evans, M. J., Chipperfield, M. P., Lewis, A. C., Hopkins, J. R., McQuaid, J. B., Watson, N., Purvis, R. M., Lee, J. D., Atlas, E. L., Blake, D. R., and Rappenglück, B.: Statistical inference of OH concentrations and air mass dilution rates from successive observations of nonmethane hydrocarbons in single air masses, Journal of Geophysical Research (Atmospheres), 112, D10S40, doi:10.1029/2006JD007594, 2007.

Bhartia, P. K., McPeters, R. D., Flynn, L. E., Taylor, S., Kramrova, N. A., Frith, S., Fisher, B., and DeLand, M.: Solar Backscatter UV (SBUV) total ozone and profile algorithm, Atmospheric Measurement Techniques, 6, 2533–2548, doi:10.5194/amt-6-2533-2013, 2013.

Box, G. E. P. and Tiao, G. C.: A Bayesian Aapproach to some outlier problems, Biometrika, 55, 119, 1968.

Carpenter, B., Gelman, A., Hoffman, M., Lee, D., Goodrich, B., Betancourt, M., Brubaker, M. A., Guo, J., Li, P., and Riddell, A.: Stan: A probabilistic programming language, Journal of Statistical Software, 20, 1–37, 2016.

Chiodo, G., Marsh, D. R., Garcia-Herrera, R., Calvo, N., and García, J. A.: On the detection of the solar signal in the tropical stratosphere, Atmospheric Chemistry & Physics, 14, 5251–5269, doi:10.5194/acp-14-5251-2014, 2014.

Cox, R. T.: Probability, frequency, and reasonable expectation, Am. Jour. Phys., 14, 1–13, 1946.

Crutzen, P. J.: Ozone production rates in an oxygen-hydrogen-nitrogen oxide atmosphere, Journal of Geophysical Research, 76, 7311, doi:10.1029/JC076i030p07311, 1971.

Damadeo, R. P., Zawodny, J. M., Thomason, L. W., and Iyer, N.: SAGE version 7.0 algorithm: application to SAGE II, Atmospheric Measurement Techniques, 6, 3539–3561, doi:10.5194/amt-6-3539-2013, 2013.

Davis, S. M., Rosenlof, K. H., Hassler, B., Hurst, D. F., Read, W. G., Vömel, H., Selkirk, H., Fujiwara, M., and Damadeo, R.: The Stratospheric Water and Ozone Satellite Homogenized (SWOOSH) database: a long-term database for climate studies, Earth System Science Data, 8, 461–490, doi:10.5194/essd-8-461-2016, 2016.

DeLand, M. T., Taylor, S. L., Huang, L. K., and Fisher, B. L.: Calibration of the SBUV version 8.6 ozone data product, Atmospheric Measurement Techniques, 5, 2951–2967, doi:10.5194/amt-5-2951-2012, 2012.

Dudok de Wit, T., Bruinsma, S., and Shibasaki, K.: Synoptic radio observations as proxies for upper atmosphere modelling, Journal of Space Weather and Space Climate, 4, A06, doi:10.1051/swsc/2014003, 2014.

Frith, S. M., Kramarova, N. A., Stolarski, R. S., McPeters, R. D., Bhartia, P. K., and Labow, G. J.: Recent changes in total column ozone based on the SBUV Version 8.6 Merged Ozone Data Set, Journal of Geophysical Research (Atmospheres), 119, 9735–9751, doi:10.1002/2014JD021889, 2014.

Froidevaux, L., Anderson, J., Wang, H.-J., Fuller, R. A., Schwartz, M. J., Santee, M. L., Livesey, N. J., Pumphrey, H. C., Bernath, P. F., Russell, III, J. M., and McCormick, M. P.: Global OZone Chemistry And Related trace gas Data records for the Stratosphere (GOZCARDS): methodology and sample results with a focus on HCl, H_2O, and O_3, Atmospheric Chemistry & Physics, 15, 10471–10507, doi:10.5194/acp-15-10471-2015, 2015.

Funke, B., Baumgaertner, A., Calisto, M., Egorova, T., Jackman, C. H., Kieser, J., Krivolutsky, A., López-Puertas, M., Marsh, D. R., Reddmann, T., Rozanov, E., Salmi, S.-M., Sinnhuber, M., Stiller, G. P., Verronen, P. T., Versick, S., von Clarmann, T., Vyushkova, T. Y., Wieters, N., and Wissing, J. M.: Composition changes after the "Halloween" solar proton event: the High Energy Particle Precipitation in the Atmosphere (HEPPA) model versus MIPAS data intercomparison study, Atmospheric Chemistry & Physics, 11, 9089–9139, doi:10.5194/acp-11-9089-2011, 2011.

Haigh, J. D.: The Role of Stratospheric Ozone in Modulating the Solar Radiative Forcing of Climate, Nature, 370, 544–+, doi:10.1038/370544a0, 1994.

Harris, N. R. P., Hassler, B., Tummon, F., Bodeker, G. E., Hubert, D., Petropavlovskikh, I., Steinbrecht, W., Anderson, J., Bhartia, P. K., Boone, C. D., Bourassa, A., Davis, S. M., Degenstein, D., Delcloo, A., Frith, S. M., Froidevaux, L., Godin-Beekmann, S., Jones, N., Kurylo, M. J., Kyrölä, E., Laine, M., Leblanc, S. T., Lambert, J.-C., Liley, B., Mahieu, E., Maycock, A., de Mazière, M., Parrish, A., Querel, R., Rosenlof, K. H., Roth, C., Sioris, C., Staehelin, J., Stolarski, R. S., Stübi, R., Tamminen, J., Vigouroux, C., Walker, K. A.,

Wang, H. J., Wild, J., and Zawodny, J. M.: Past changes in the vertical distribution of ozone - Part 3: Analysis and interpretation of trends, Atmospheric Chemistry & Physics, 15, 9965–9982, doi:10.5194/acp-15-9965-2015, 2015.

Hassler, B., Petropavlovskikh, I., Staehelin, J., August, T., Bhartia, P. K., Clerbaux, C., Degenstein, D., De Mazière, M., Dinelli, B. M., Dudhia, A., Dufour, G., Frith, S. M., Froidevaux, L., Godin-Beekmann, S., Granville, J., Harris, N. R. P., Hoppel, K., Hubert, D., Kasai, Y., Kurylo, M. J., Kyrölä, E., Lambert, J.-C., Levelt, P. F., McElroy, C. T., McPeters, R. D., Munro, R., Nakajima, H., Parrish, A., Raspollini, P., Remsberg, E. E., Rosenlof, K. H., Rozanov, A., Sano, T., Sasano, Y., Shiotani, M., Smit, H. G. J., Stiller, G., Tamminen, J., Tarasick, D. W., Urban, J., van der A, R. J., Veefkind, J. P., Vigouroux, C., von Clarmann, T., von Savigny, C., Walker, K. A., Weber, M., Wild, J., and Zawodny, J. M.: Past changes in the vertical distribution of ozone - Part 1: Measurement techniques, uncertainties and availability, Atmospheric Measurement Techniques, 7, 1395–1427, doi:10.5194/amt-7-1395-2014, 2014.

Hubert, D., Lambert, J.-C., Verhoelst, T., Granville, J., Keppens, A., Baray, J.-L., Bourassa, A. E., Cortesi, U., Degenstein, D. A., Froidevaux, L., Godin-Beekmann, S., Hoppel, K. W., Johnson, B. J., Kyrölä, E., Leblanc, T., Lichtenberg, G., Marchand, M., McElroy, C. T., Murtagh, D., Nakane, H., Portafaix, T., Querel, R., Russell, III, J. M., Salvador, J., Smit, H. G. J., Stebel, K., Steinbrecht, W., Strawbridge, K. B., Stübi, R., Swart, D. P. J., Taha, G., Tarasick, D. W., Thompson, A. M., Urban, J., van Gijsel, J. A. E., Van Malderen, R., von der Gathen, P., Walker, K. A., Wolfram, E., and Zawodny, J. M.: Ground-based assessment of the bias and long-term stability of 14 limb and occultation ozone profile data records, Atmos. Meas. Tech., 9, 2497–2534, doi:10.5194/amt-9-2497-2016, 2016.

Johnston, H.: Reduction of Stratospheric Ozone by Nitrogen Oxide Catalysts from Supersonic Transport Exhaust, Science, 173, 517–522, doi:10.1126/science.173.3996.517, 1971.

Kidston, J., Scaife, A. A., Hardiman, S. C., Mitchell, D. M., Butchart, N., Baldwin, M. P., and Gray, L. J.: Stratospheric influence on tropospheric jet streams, storm tracks and surface weather, Nature Geoscience, 8, 433–440, doi:10.1038/ngeo2424, 2015.

Kirgis, G., Leblanc, T., McDermid, I. S., and Walsh, T. D.: Stratospheric ozone interannual variability (1995-2011) as observed by lidar and satellite at Mauna Loa Observatory, HI and Table Mountain Facility, CA, Atmospheric Chemistry & Physics, 13, 5033–5047, doi:10.5194/acp-13-5033-2013, 2013.

Kramarova, N. A., Bhartia, P. K., Frith, S. M., McPeters, R. D., and Stolarski, R. S.: Interpreting SBUV smoothing errors: an example using the quasi-biennial oscillation, Atmospheric Measurement Techniques, 6, 2089–2099, doi:10.5194/amt-6-2089-2013, 2013a.

Kramarova, N. A., Frith, S. M., Bhartia, P. K., McPeters, R. D., Taylor, S. L., Fisher, B. L., Labow, G. J., and DeLand, M. T.: Validation of ozone monthly zonal mean profiles obtained from the version 8.6 Solar Backscatter Ultraviolet algorithm, Atmospheric Chemistry & Physics, 13, 6887–6905, doi:10.5194/acp-13-6887-2013, 2013b.

Krueger, A. J., Guenther, B., Fleig, A. J., Heath, D. F., Hilsenrath, E., McPeters, R., and Prabhakara, C.: Satellite ozone measurements, Philosophical Transactions of the Royal Society of London Series A, 296, 191–204, doi:10.1098/rsta.1980.0164, 1980.

Kuchar, A., Sacha, P., Miksovsky, J., and Pisoft, P.: The 11-year solar cycle in current reanalyses: a (non)linear attribution study of the middle atmosphere, Atmos. Chem. Phys., 15, 6879–6895, doi:10.5194/acp-15-6879-2015, 2015.

Kyrölä, E., Laine, M., Sofieva, V., Tamminen, J., Päivärinta, S.-M., Tukiainen, S., Zawodny, J., and Thomason, L.: Combined SAGE II-GOMOS ozone profile data set for 1984-2011 and trend analysis of the vertical distribution of ozone, Atmospheric Chemistry & Physics, 13, 10 645–10 658, doi:10.5194/acp-13-10645-2013, 2013.

Labow, G. J., McPeters, R. D., Bhartia, P. K., and Kramarova, N.: A comparison of 40 years of SBUV measurements of column ozone with data from the Dobson/Brewer network, Journal of Geophysical Research (Atmospheres), 118, 7370–7378, doi:10.1002/jgrd.50503, 2013.

Laine, M., Latva-Pukkila, N., and Kyrölä, E.: Analysing time-varying trends in stratospheric ozone time series using the state space approach, Atmospheric Chemistry & Physics, 14, 9707–9725, doi:10.5194/acp-14-9707-2014, 2014.

Lee, T. C. K., Zwiers, F. W., Hegerl, G. C., Zhang, X., and Tsao, M.: A Bayesian Climate Change Detection and Attribution Assessment., Journal of Climate, 18, 2429–2440, doi:10.1175/JCLI3402.1, 2005.

Maycock, A. C., Matthes, K., Tegtmeier, S., Thiéblemont, R., and Hood, L.: The representation of solar cycle signals in stratospheric ozone - Part 1: A comparison of recently updated satellite observations, Atmospheric Chemistry & Physics, 16, 10 021–10 043, doi:10.5194/acp-16-10021-2016, 2016.

McLinden, C. A., Tegtmeier, S., and Fioletov, V.: Technical Note: A SAGE-corrected SBUV zonal-mean ozone data set, Atmospheric Chemistry & Physics, 9, 7963–7972, 2009.

McPeters, R. D., Bhartia, P. K., Haffner, D., Labow, G. J., and Flynn, L.: The version 8.6 SBUV ozone data record: An overview, Journal of Geophysical Research (Atmospheres), 118, 8032–8039, doi:10.1002/jgrd.50597, 2013.

Mironova, I. A., Aplin, K. L., Arnold, F., Bazilevskaya, G. A., Harrison, R. G., Krivolutsky, A. A., Nicoll, K. A., Rozanov, E. V., Turunen, E., and Usoskin, I. G.: Energetic Particle Influence on the Earth's Atmosphere, Space Science Reviews, 194, 1–96, doi:10.1007/s11214-015-0185-4, 2015.

Molina, M. J. and Rowland, F. S.: Stratospheric sink for chlorofluoromethanes: chlorine atomc-atalysed destruction of ozone, Nature, 249, 810–812, doi:10.1038/249810a0, 1974.

Nair, P. J., Godin-Beekmann, S., Froidevaux, L., Flynn, L. E., Zawodny, J. M., Russell, III, J. M., Pazmiño, A., Ancellet, G., Steinbrecht, W., Claude, H., Leblanc, T., McDermid, S., van Gijsel, J. A. E., Johnson, B., Thomas, A., Hubert, D., Lambert, J.-C., Nakane, H., and Swart, D. P. J.: Relative drifts and stability of satellite and ground-based stratospheric ozone profiles at NDACC lidar stations, Atmospheric Measurement Techniques, 5, 1301–1318, doi:10.5194/amt-5-1301-2012, 2012.

Nazaryan, H. and McCormick, M. P.: Comparisons of Stratospheric Aerosol and Gas Experiment (SAGE II) and Solar Backscatter Ultraviolet Instrument (SBUV/2) ozone profiles and trend estimates, Journal of Geophysical Research (Atmospheres), 110, D17302, doi:10.1029/2004JD005483, 2005.

Neal, R. M.: Probabilistic inference using Markov chain Monte Carlo methods, 1993.

Newman, P. A., Nash, E. R., and Rosenfield, J. E.: What controls the temperature of the Arctic stratosphere during the spring?, Journal of Geophysical Research, 106, 19 999–20 010, doi:10.1029/2000JD000061, 2001.

1270   Polvani, L. M., Waugh, D. W., Correa, G. J. P., and Son, S.-W.: Stratospheric Ozone Depletion: The Main Driver of Twentieth-Century Atmospheric Circulation Changes in the Southern Hemisphere, Journal of Climate, 24, 795–812, doi:10.1175/2010JCLI3772.1, 2011.

Robock, A.: Volcanic eruptions and climate, Reviews of Geophysics, 38, 191–219, doi:10.1029/1998RG000054, 2000.

1275   Sato, M., Hansen, J. E., McCormick, M. P., and Pollack, J. B.: Stratospheric aerosol optical depths, 1850-1990, Journal of Geophysical Research: Atmospheres, 98, 22 987–22 994, doi:10.1029/93JD02553, http://dx.doi.org/10.1029/93JD02553, 1993.

Shepherd, T. G., Plummer, D. A., Scinocca, J. F., Hegglin, M. I., Fioletov, V. E., Reader, M. C., Remsberg, E., von Clarmann, T., and Wang, H. J.: Reconciliation of halogen-induced ozone loss with the total-column

1280   ozone record, Nature Geoscience, 7, 443–449, doi:10.1038/ngeo2155, 2014.

Sioris, C. E., McLinden, C. A., Fioletov, V. E., Adams, C., Zawodny, J. M., Bourassa, A. E., Roth, C. Z., and Degenstein, D. A.: Trend and variability in ozone in the tropical lower stratosphere over 2.5 solar cycles observed by SAGE II and OSIRIS, Atmospheric Chemistry & Physics, 14, 3479–3496, doi:10.5194/acp-14-3479-2014, 2014.

1285   Sofieva, V. F., Rahpoe, N., Tamminen, J., Kyrölä, E., Kalakoski, N., Weber, M., Rozanov, A., von Savigny, C., Laeng, A., von Clarmann, T., Stiller, G., Lossow, S., Degenstein, D., Bourassa, A., Adams, C., Roth, C., Lloyd, N., Bernath, P., Hargreaves, R. J., Urban, J., Murtagh, D., Hauchecorne, A., Dalaudier, F., van Roozendael, M., Kalb, N., and Zehner, C.: Harmonized dataset of ozone profiles from satellite limb and occultation measurements, Earth System Science Data, 5, 349–363, doi:10.5194/essd-5-349-2013, 2013.

1290   Sofieva, V. F., Kalakoski, N., Päivärinta, S.-M., Tamminen, J., Laine, M., and Froidevaux, L.: On sampling uncertainty of satellite ozone profile measurements, Atmospheric Measurement Techniques, 7, 1891–1900, doi:10.5194/amt-7-1891-2014, 2014.

Solomon, S., Ivy, D. J., Kinnison, D., Mills, M. J., Neely, R. R., and Schmidt, A.: Emergence of healing in the Antarctic ozone layer, Science, 353, 269–274, doi:10.1126/science.aae0061, 2016.

1295   Soukharev, B. E. and Hood, L. L.: Solar cycle variation of stratospheric ozone: Multiple regression analysis of long-term satellite data sets and comparisons with models, Journal of Geophysical Research (Atmospheres), 111, D20314, doi:10.1029/2006JD007107, 2006.

Staehelin, J., Renaud, A., Bader, J., McPeters, R., Viatte, P., Hoegger, B., Bugnion, V., Giroud, M., and Schill, H.: Total ozone series at Arosa (Switzerland): Homogenization and data comparison, Journal of Geophysical

1300   Research, 103, 5827–5841, doi:10.1029/97JD02402, 1998.

Tiao, G. C., Xu, D., Pedrick, J. H., Zhu, X., and Reinsel, G. C.: Effects of autocorrelation and temporal sampling schemes on estimates of trend and spatial correlation, Journal of Geophysical Research, 95, 20 507–20 517, doi:10.1029/JD095iD12p20507, 1990.

Toohey, M., Hegglin, M. I., Tegtmeier, S., Anderson, J., Añel, J. A., Bourassa, A., Brohede, S., Degenstein,

1305   D., Froidevaux, L., Fuller, R., Funke, B., Gille, J., Jones, A., Kasai, Y., Krüger, K., Kyrölä, E., Neu, J. L., Rozanov, A., Smith, L., Urban, J., Clarmann, T., Walker, K. A., and Wang, R. H. J.: Characterizing sampling biases in the trace gas climatologies of the SPARC Data Initiative, Journal of Geophysical Research (Atmospheres), 118, 11, doi:10.1002/jgrd.50874, 2013.

Tummon, F., Hassler, B., Harris, N. R. P., Staehelin, J., Steinbrecht, W., Anderson, J., Bodeker, G. E., Bourassa,
1310   A., Davis, S. M., Degenstein, D., Frith, S. M., Froidevaux, L., Kyrölä, E., Laine, M., Long, C., Penckwitt,
A. A., Sioris, C. E., Rosenlof, K. H., Roth, C., Wang, H.-J., and Wild, J.: Intercomparison of vertically re-
solved merged satellite ozone data sets: interannual variability and long-term trends, Atmospheric Chemistry
& Physics, 15, 3021–3043, doi:10.5194/acp-15-3021-2015, 2015.

Wang, H. J., Cunnold, D. M., Thomason, L. W., Zawodny, J. M., and Bodeker, G. E.: Assessment of
1315   SAGE version 6.1 ozone data quality, Journal of Geophysical Research (Atmospheres), 107, 4691,
doi:10.1029/2002JD002418, 2002.

Wild, J. D. and Long, C. S.: A Coherent Ozone Profile Dataset from SBUV, SBUV/2: 1979 to 2016, in prepa-
ration, 2017.

WMO: Scientific Assessment of Ozone Depletion: 2010, Global Ozone Research and Monitoring Project, 52,
1320   516, 2011.

WMO: Scientific Assessment of Ozone Depletion: 2014 Global Ozone Research and Monitoring Project Re-
port, World Meteorological Organization, p. 416, geneva, Switzerland, 2014.

WMO/UNEP: Scientific Assessment of Ozone Depletion: 1994, World Meteorological Organization, geneva,
Switzerland, 1994.